Overflow metabolism in *E. coli* results from efficient proteome allocation

Markus Basan, Sheng Hui, Hiroyuki Okano, Zhongge Zhang, Yang Shen, James R. Williamson and Terence Hwa

Supplementary Information

Table of Contents

Supplementary Note 1: Proteome allocation model of acetate overflow

In this note, we describe the model introduced in the main text in detail. The main equations of the model are already found in the main text, but are again presented here with further explanations. We then apply these equations to the data collected and deduce the parameters.

A. Model Description

We construct a mathematical model of balanced growth of *E. coli* similar to previous works[1-3], taking into account energy production via fermentation and respiration. Energy biogenesis via the fermentation pathway mainly refers to glycolysis, including the decarboxylation of pyruvate and the conversion of acetyl-coA to acetate (Extended Data Figure 2a), whereas energy biogenesis via respiration refers to the full oxidation of carbon via the combination of glycolysis and TCA (Extended Data Figure 2b). While there are alternative energy biogenesis pathways such as the pentose phosphate pathway, the Entner-Doudoroff pathway, and the recently discovered PEP-glyoxylate cycle[4], either their usage is negligible in the growth conditions we considered or they have small effect on our results, as demonstrated in Supplementary Note 4.

A1. Energy flux balance: At steady state, the energy demand (J_E) is equal to the energy flux generated by fermentation ($J_{E,f}$) and respiration pathway ($J_{E,r}$), or

$$J_{E,f} + J_{E,r} = J_E . \qquad [S1]$$

Assuming a linear dependence of energy demand on growth rate, i.e.,

$$J_E(\lambda) = \sigma\lambda . \qquad [S2]$$

where σ is the coefficient relating growth rate λ to energy demand,[1] we have

$$J_{E,f} + J_{E,r} = \sigma\lambda . \qquad [S3]$$

A2. Proteome constraint: The proteome fractions of the two pathways are denoted by ϕ_f and ϕ_r respectively and are under the proteome constraint that

$$\phi_f + \phi_r + \phi_{BM} = 1 , \qquad [S4]$$

where ϕ_{BM} denotes the proteome fraction of all proteins outside of those used for energy biogenesis, including ribosomes, biosynthesis pathways, etc. Motivated by previous results[1-3], we assume a linear dependence on growth rate λ for ϕ_{BM} ,

$$\phi_{BM} = \phi_0 + b\lambda . \qquad [S5]$$

[1] The energy flux produced by precursor generating pathways is proportional to λ and can therefore be absorbed into the coefficient σ .

It is convenient to introduce $\phi_{E,\max} = 1 - \phi_0$, which is the maximal proteome fraction the energy sector ($\phi_f + \phi_r$) can take on (extrapolated[2] to $\lambda = 0$). Together with the linear dependences[3] assumed for the energy flux generated by fermentation and respiration pathways respectively,

$$\begin{aligned} J_{E,f} &= \varepsilon_f \cdot \phi_f \\ J_{E,r} &= \varepsilon_r \cdot \phi_r \end{aligned}, \qquad \text{[S6]}$$

where the coefficients ε_f and ε_r are the energy production rates per unit of protein mass invested in the respective pathway (referred to as "proteome efficiency" in the main text), Eq. [S*4*] becomes

$$\frac{J_{E,f}}{\varepsilon_f} + \frac{J_{E,r}}{\varepsilon_r} = \phi_{E,\max} - b \cdot \lambda \,. \qquad \text{[S7]}$$

For the simple relation between fluxes and enzyme abundances given by Eq. [S6] to hold in varying steady-state conditions, the ratios between the abundances of enzymes constituting the respective pathways should be fixed. However, proteomics data from this work and a previous publication[3] validates this assumption. Furthermore, the assumed behavior arises naturally from the optimization of protein cost for a given flux[5].

A3. Carbon flux balance: Eqs. [S*3*] and [S*7*] are complemented by an equation balancing the total carbon uptake flux $J_{C,in}$ to the carbon flux for biosynthesis ($J_{C,BM}$) and for energy biogenesis via the fermentation and respiration pathway ($J_{C,f}$ and $J_{C,r}$ respectively), i.e.,

$$J_{C,BM} + J_{C,f} + J_{C,r} = J_{C,in} \,. \qquad \text{[S8]}$$

The biosynthesis flux (i.e., the flux devoted to the production of precursors) is proportional to the growth rate given fixed stoichiometry of metabolic network[6,7], written as,

$$J_{C,BM} = \beta \cdot \lambda \,, \qquad \text{[S9]}$$

with a proportionality constant β. The carbon flux and energy flux for each pathway are related via biochemical stoichiometry,

$$\begin{aligned} J_{E,f} &= e_f \cdot J_{C,f} \\ J_{E,r} &= e_r \cdot J_{C,r} \end{aligned}, \qquad \text{[S10]}$$

with proportionality constants e_f, e_r (referred to as "carbon efficiency" in the main text). Together, we have

---

[2] Note that this does not mean that the growth-rate dependence of $\phi_f + \phi_r$ will continue in the form given below for all λ down to $\lambda = 0$. As discussed below, the applicability of the model is for $\lambda \geq \lambda_{ac}$ where acetate is excreted.

[3] We point out that the proportionalities between fluxes and the corresponding proteome sectors of the metabolic pathway are based on empirical evidence[11]. In particular, this model encompasses, but does not depend on much stronger assumptions like saturation of involved enzymes or approximately constant metabolite concentrations.

$$\frac{J_{E,f}}{e_f} + \frac{J_{E,r}}{e_r} = J_{C,in} - \beta\lambda \,. \qquad [S11]$$

The carbon uptake flux $J_{C,in}$ is set by growth conditions: it can be varied by using different carbon substrates or by directly dialing the expression level of specific carbon uptake system as described in the main text. Together, Eqs. [S*3*], [S*7*], and [S*11*] form a complete set of equations from which the growth rate λ and the energy fluxes $J_{E,f}$ and $J_{E,r}$ are determined, subject to the values of the 8 parameters, whose estimates will be described in Sec. D below. For given conversion factors between redox molecules (e.g., NADH, NADPH, $FADH_2$) and ATP molecule, the values of e_f and e_r are determined by the chemical stoichiometry based on the processes described in Extended Data Figure 2; see Sec. D1 of this Note for details. The remaining parameters are determined by comparing the proteome fractions obtained from Mass Spec analysis and flux estimates based on the measurements of rates of acetate excretion, CO_2 evolution, and biomass growth under a range of growth conditions.

B. Model Solution

Formally, the growth-rate dependences of the proteome fractions $J_{E,f}(\lambda)$ and $J_{E,r}(\lambda)$ are obtained from Eqs. [S*3*], [S*7*], and [S*11*] implicitly from their dependences on the carbon uptake flux $J_{C,in}$, e.g., $J_{E,f}(\lambda)$ is obtained from $J_{E,f}(J_{C,in})$ and $\lambda(J_{C,in})$. In practice, these relations can be easily obtained by simply eliminating the dependences on $J_{C,in}$, e.g., solving for $J_{E,f}(\lambda)$ and $J_{E,r}(\lambda)$ using Eqs. [S*3*] and [S*7*], without ever using Eq. [S*11*]. Thus, we find

$$J_{E,f} = \varepsilon_f \frac{\left(\sigma/\varepsilon_r + b\right)\lambda - \phi_{E,\max}}{\left(\varepsilon_f/\varepsilon_r\right) - 1}, \qquad [S12]$$

$$J_{E,r} = \varepsilon_r \frac{-\left(\sigma/\varepsilon_f + b\right)\lambda + \phi_{E,\max}}{1 - \left(\varepsilon_r/\varepsilon_f\right)}. \qquad [S13]$$

According to the main hypothesis of this paper, the protein cost of energy generation via fermentation is lower than that of respiration: $\varepsilon_f > \varepsilon_r$. Under this condition, as the growth rate increases the respiration energy flux decreases with increasing growth rate, and a larger fraction of energy is generated via fermentation. The solution is clearly not valid where either $J_{E,f}$ or $J_{E,r}$ takes on negative values; this restricts the solution to an intermediate range of λ as discussed below.

The rate of acetate excretion is simply given by the flux through the fermentation pathway, $J_{ac} = S_{ac} J_{C,f} = S_{ac} \frac{J_{E,f}}{e_f}$, where $S_{ac} = 1/3$ from the stoichiometry of the molecules involved[4]. Thus

$$J_{ac} = S_{ac} \frac{\varepsilon_f}{e_f} \frac{\left(\sigma/\varepsilon_r + b\right)\lambda - \phi_{E,\max}}{\left(\varepsilon_f/\varepsilon_r\right) - 1}, \qquad \text{[S14]}$$

which captures the threshold-linear form observed in Figure 1 of the main text (described by Eq. [1]), with the threshold growth rate

$$\lambda_{ac} = \frac{\phi_{E,\max}}{\left(\sigma/\varepsilon_r\right) + b}, \qquad \text{[S15]}$$

and a slope given by

$$s_{ac} = S_{ac} \frac{\varepsilon_f}{e_f} \frac{\sigma/\varepsilon_r + b}{\left(\varepsilon_f/\varepsilon_r\right) - 1}. \qquad \text{[S16]}$$

Similarly, the respiration fraction can be read out by the CO_2 evolution rate, whose respiratory component $J_{CO_2,r}$ is given by $J_{CO_2,r} = S_{CO_2,r} J_{C,r} = S_{CO_2,r} \frac{J_{E,r}}{e_r}$, where $S_{CO_2,r} = 1/6$. Thus

$$J_{CO_2,r} = S_{CO_2,r} \frac{\varepsilon_r}{e_r} \frac{\phi_{E,\max} - \left(\sigma/\varepsilon_f + b\right)\lambda}{1 - \left(\varepsilon_r/\varepsilon_f\right)}, \qquad \text{[S17]}$$

which captures the respiratory CO_2 line shown in Extended Data Figure 3a, with the threshold growth rate given by

$$\lambda_{CO_2,r} = \frac{\phi_{E,\max}}{\left(\sigma/\varepsilon_f\right) + b}, \qquad \text{[S18]}$$

and the slope

$$s_{CO_2,r} = -S_{CO_2,r} \frac{\varepsilon_r}{e_r} \frac{\sigma/\varepsilon_f + b}{1 - \left(\varepsilon_r/\varepsilon_f\right)}. \qquad \text{[S19]}$$

Eqs. [S*14*]-[S*19*] are the major outcome of the model, with Eqs. [S*14*] and [S*17*] describing the threshold-linear forms of the growth-rate dependent acetate excretion and CO_2 evolution (illustrated in Figure N1), and Eqs. [S*15*]-[S*16*] and [S*18*]-[S*19*] describing the key phenomenological parameters ($\lambda_{ac}, s_{ac}, \lambda_{CO_2,r}, s_{CO_2,r}$) in terms of the model parameters. In the remainder of this Note, we will describe approaches to test these model predictions. In Sec. C, we will describe various perturbations, which change the values of the model parameters, and see how they affect the model predictions. In Sec. D, we will directly estimate the values of the

[4] Here, $S_{ac} = 1/3$ simply because of the chemical reaction 6C → 2Acetate + 2CO_2 of the fermentation pathway: the carbon uptake flux $J_{C,f}$ measured in units of the number of carbon atoms (C), is 3 times of the flux of acetate molecules.

model parameters for wild-type cells and compare them to the measured values of the phenomenlogical parameters. However, before we close this section, we make a note that our empirical results on the location of the acetate and CO_2 lines already provide important constraints on the key parameters ε_f and ε_r.

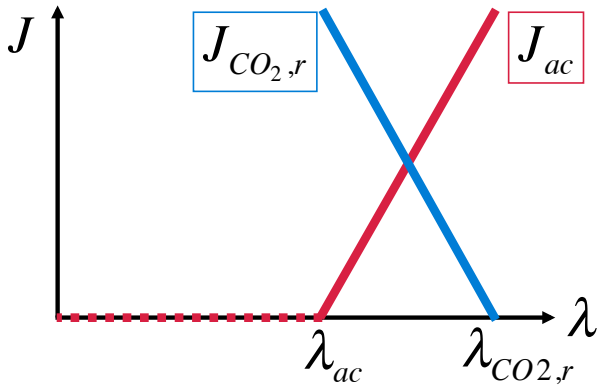

Figure N1: Illustration of model behavior for carbon limitation. Under carbon limitation, the model predicts a linear decrease of the acetate excretion rate with decreasing growth rate, which vanishes at a threshold growth rate λ_{ac}. The corresponding experimental data is presented in Figure 1 of the main text. Correspondingly, the model predicts a linear increase of the respiration CO_2 evolution rate with decreasing growth rate, with experimental data presented in Extended Data Figure 3a.

We note that the model is only self-consistent if the solutions (energy fluxes) are non-negative. Given the solutions illustrated in Figure N1, the applicable range of the model is in the growth rate range $\lambda_{ac} \le \lambda \le \lambda_{CO_2,r}$, which is just sufficient to describe the regime of acetate excretion, the goal of this study. In practice, the experimental value of $\lambda_{CO_2,r}$ (Extended Data Figure 3a) well exceeds the largest growth rate attainable in minimal medium. Hence the upper bound is never exceeded. For $\lambda < \lambda_{ac}$, $J_{E,f} = 0$ and the proteome fractions described here are no longer constrained to allow a determination of $J_{E,r}$.

Also, with the knowledge of location of the acetate and the CO_2 lines (i.e., the values of λ_{ac} and $\lambda_{CO_2,r}$), it is already possible to draw quantitative conclusions regarding the key parameters ε_f, ε_r, which describe the proteome efficiencies of the two energy biogenesis pathways and are of central importance to our model. From Eqs. [S*15*] and [S*18*], we obtain

$$\frac{\lambda_{ac}}{\lambda_{CO_2,r}} = \frac{\left(\sigma/\varepsilon_f\right)+b}{\left(\sigma/\varepsilon_r\right)+b}. \qquad \text{[S20]}$$

Because $\lambda_{ac} < \lambda_{CO_2,r}$, we have $\sigma/\varepsilon_f < \sigma/\varepsilon_r$. Then from Eq. [S*20*] we can obtain a lower bound

$$\frac{\lambda_{ac}}{\lambda_{CO_2,r}} \ge \frac{\sigma/\varepsilon_f}{\sigma/\varepsilon_r} = \frac{\varepsilon_r}{\varepsilon_f}. \qquad \text{[S21]}$$

Using the empirically determined values for λ_{ac} and $\lambda_{CO_2,r}$ (Figure 1 and Extended Data Figure 3a, respectively), we then obtain a lower bound for the ratio of the two energy production efficiencies

$$\frac{\varepsilon_f}{\varepsilon_r} \geq 1.5 \,. \qquad \text{[S22]}$$

Hence, we conclude that the proteome efficiency of energy biogenesis by fermentation must be at least 50% higher than the corresponding efficiency by respiration. Note that this conclusion does not depend on the direct determination of the efficiency paramters to be described in Sec. D.

C. Model Predictions and Response to Perturbations

To test the model predictions, particularly the dependences of the acetate line Eq. [S*14*] on the model parameters, we derive the response of the model to a set of well-defined perturbations. Before discussing each specific case, it is worth summarizing the different classes of relevant perturbations the model admits. The parameters ε_f, ε_r, e_f, e_r describing inherent properties of the pathways are hard-wired in central metabolism and difficult to change. The remainders are

1. perturbations in carbon flux available for energy biogenesis, $J_{C,in} - J_{C,BM}$;
2. perturbations in proteome fraction available for energy biogenesis, $\phi_{BM}(\lambda)$;
3. perturbations in energy consumption $J_E(\lambda)$.

We designed multiple approaches to alter each of these three classes of perturbations. The first class affecting the carbon flux is referred to as "carbon limitation". This can be achieved by growing cells on different carbon sources, on low concentrations of carbon substrates in a chemostat, titrating the expression level of carbon transporters (thereby directly changing $J_{C,in}$), or by adding precursors to the medium lowering the demand for biomass production (lowering β). Effects of these perturbations on acetate excretion are summarized in Figure 1 of the main text. The second class is referred to as "proteome limitation". It is achieved by expressing large quantities of useless protein or adding antibiotics that interfere with ribosomal efficiency. Effects of these perturbations on acetate excretion are given in Figure 2 and Figure 3a,b,c of the main text. The third class of perturbations is referred to as "energy limitation". This group encompasses all perturbations directly affecting energy expenditure by the cell, and is realized in our experiments by introducing futile cycles that leak protons across the inner cell membrane. The effects of these perturbations on acetate excretion are given in Figure 3d.

C1. Carbon Limitation: In our model, the effect of this perturbation on the acetate line (Eq. [S*14*]) is very simple: In deriving Eq. [S*14*], Eq. [S*11*] relating carbon uptake ($J_{C,in}$) and expenditure for biosynthesis ($J_{C,BM} = \beta \cdot \lambda$) to growth rate was not used. Hence, the form of Eq. [S*14*] remains unchanged, independent of the values of $J_{C,in}$ and $J_{C,BM}$. What this implies is that by either controlling the carbon uptake rate (changing $J_{C,in}$) or providing precursors in the

medium (changing β), the corresponding rate of acetate excretion should fall on the *same* line given by Eq. [S*14*]. Similarly, the model predicts the respiratory CO_2 evolution rate to fall on the same line given by Eq. [S*17*] in response to these perturbations. Equivalently, we expect gene expression of the energy sectors (ϕ_f, ϕ_r) to exhibit the same patterns, as given by Eqs. [S*12*] and [S*13*] in combination with Eq. [S*6*], under these perturbations. While the biosynthesis pathways of these 7 amino acids were estimated to be 9.3% of the total proteome for cells grown in glucose minimal medium, the proteomic response for the addition of non-degradable amino acids is part of the general response to carbon limitation, characterized by Eq. [S5]. The proteomic changes follow the response associated with carbon limitation, because 'carbon availability' sensed by the cell is affected directly by the addition of these amino acids, as these amino acid pools are in equilibrium with the corresponding ketoacids pools due to the reversible trans-amination reactions[8], such that increases in amino acids pools lead to corresponding increases in ketoacid pools, which in turn inhibit the synthesis of cAMP[2], the major sensor of carbon availability and a global regulator of gene expression.

C2. Proteome Limitation: Perturbations in proteome allocation, which decrease the proteome fraction available for energy biogenesis, have a distinctly different effect from carbon limitation. There are several possibilities how this kind of perturbation can be implemented experimentally. One is the induced expression of large quantities of useless proteins, which directly decreases the proteome fraction available for other sectors[3]. An alternative is to apply antibiotics that directly interfere with ribosomal function thereby requiring a larger fraction of the proteome to be allocated to ribosomes in order to sustain a specific growth rate[6].

Following previous studies[1,3], we express large amounts of LacZ as the "useless protein. The absolute abundance of LacZ is readily characterized, and its proteome fraction is denoted as ϕ_Z. The existence of an additional proteome sector ϕ_Z reduces the proteome fraction available for the remaining sectors of the proteome. From previous works[1-3], we know that the growth-rate dependent fractions $\phi_i(\lambda)$ which sum up to a fraction $\phi_{\max}$ of approximately 50%, with the other 50% being growth-rate independent. The effect of expressing useless proteins (ϕ_Z) can be modeled by reducing the growth-rate dependent fraction from $\phi_{\max}$ to $\phi_{\max} - \phi_Z$, which amounts to 'compressing' each growth-rate dependent fractions equally from $\phi_i(\lambda)$ to $\phi_i(\lambda)\cdot[1-\phi_Z/\phi_{\max}]$; see Hui et al[3] for a direct validation of this result using proteomic analysis.

Applying these results to the proteome fractions for the energy generating pathways, we have

$$\phi_f(\phi_Z) = \phi_f(\phi_Z = 0)\cdot[1-\phi_Z/\phi_{\max}], \qquad \text{[S23]}$$

and

$$\phi_r(\phi_Z) = \phi_r(\phi_Z = 0)\cdot[1-\phi_Z/\phi_{\max}]. \qquad \text{[S24]}$$

The prediction Eq. [S*23*] is validated by the data presented in Extended Data Figure 4a, which shows that acetate excretion rate (which is a read out of ϕ_f) is indeed reduced linearly upon increasing the expression of LacZ.

To see how the expression of useless proteins generally affects our model, we assume that (a) the fundamental relations leading to Eqs. [S*3*], [S*7*], [S*11*], i.e. proteome constraint (Eq. [S*4*]) and flux balance (Eqs. [S*1*], [S*8*]), are unaffected by the useless proteins, and (b) the model parameters relating the energy fluxes to either the required proteome fractions or the carbon fluxes are also unaffected (because these relations are derived from enzyme properties). Given Eqs. [S*23*]and [S*24*], together with Eq. [S*6*], the balance of energy flux (Eq. [S*3*]) implies that the growth rate must be reduced to[5]

$$\lambda(\phi_Z) = \lambda(\phi_Z = 0)\cdot[1-\phi_Z/\phi_{\max}]. \qquad \text{[S25]}$$

Eq. [S*25*] is a general result of the effect of useless protein expression, first demonstrated for cells grown in a set of rich medium in Scott et al[1], and is verified in this work for growth in a number of minimal medium; see Extended Data Figure 4. The data suggest a value of $\phi_{\max} \approx 0.42$, which is consistent with the previous studies[1-3]. A corollary of Eqs. [S*23*]-[S*25*] is that

$$\phi_f(\phi_Z)/\phi_f(\phi_Z = 0) = \lambda(\phi_Z)/\lambda(\phi_Z = 0), \qquad \text{[S26]}$$

$$\phi_r(\phi_Z)/\phi_r(\phi_Z = 0) = \lambda(\phi_Z)/\lambda(\phi_Z = 0), \qquad \text{[S27]}$$

The linearity between ϕ_f and the growth rate upon changes in useless protein expression is vividly shown in Figure 2a, with the acetate flux taken as the readout of ϕ_f.

Next, applying Eqs. [S*23*]-[S*25*] to the proteome constaint Eq. [S*4*], we see that the parameter $\phi_{E,\max}$ is similarly reduced upon the expression of useless proteins, i.e.,

$$\phi_{E,\max}(\phi_Z) = \phi_{E,\max}\cdot[1-\phi_Z/\phi_{\max}], \qquad \text{[S28]}$$

Provided that $J_{C,in}(\phi_Z)$ is also scaled by the factor $[1-\phi_Z/\phi_{\max}]$, i.e.,

$$J_{C,in}(\phi_Z) = J_{C,in}(\phi_Z = 0)\cdot[1-\phi_Z/\phi_{\max}], \qquad \text{[S29]}$$

then Eqs. [S*3*], [S*7*], and [S*11*] describe the relation between ϕ_f, ϕ_r, and λ for any ϕ_Z. Consequently, the solution is still given by Eqs. [S*12*]-[S*19*], i.e., acetate excretion still follows the acetate line (Eq. [S*14*]) and CO_2 evolution still follows the CO_2 line (Eq. [S*17*]), except that the phenomenological parameters (the threshold and slope) now depend on the degree of useless protein expression, ϕ_Z, through $\phi_{E,\max}(\phi_Z)$ given in Eq. [S*28*]. Thus for acetate excretion, the model predicts

$$J_{ac} = S_{ac}\frac{\varepsilon_f}{e_f}\frac{\left(\sigma/\varepsilon_r + b\right)\lambda - \phi_{E,\max}\cdot[1-\phi_Z/\phi_{\max}]}{\left(\varepsilon_f/\varepsilon_r\right)-1}, \qquad \text{[S30]}$$

[5] Alternatively, we can use the empirical result shown in Figure N5 to justify the linear dependence of the cell's energy demand, i.e., $J_E = \sigma\cdot\lambda$, up to a small maintenance energy allowed by the small deviation of data from Eq. [S27].

which is a line with the threshold λ_{ac} linearly shifted by $\phi_Z / \phi_{\max}$ but with the slope unaffected. This is illustrated in Figure N2a, with the expression of useless protein resulting in a *parallel* shift of the acetate line to the left, by an amount determined by $\phi_Z / \phi_{\max}$. The parallel shift is indeed observed in Figure 3a, and the linear dependence of λ_{ac} on $\phi_Z / \phi_{\max}$ is captured by the cyan line in Figure 2b.

Another method, which we used to generate proteome limitation was to apply the antibiotic chloramphenicol, which leads to a decrease in the translation rate which amounts to an increase in the coefficient *b* in the linear growth rate dependence of $\phi_{BM}(\lambda)$ [1]. [Chloramphenicol had been reported to inhibit respiration[9], but this had been determined to arise from Chloramphenicol's effect on mitochondria[10] and is hence not relevant to this study.] Eq. [S*14*] then predicts an increase in the slope of the acetate line (but not the y-intercept), as illustrated in Figure N2b. Note that the threshold growth rate also decreased in the case of chloramphenicol, but unlike the expression of useless proteins, the slope also increased. These predictions are in agreement with the experimental data shown in Figure 3c.

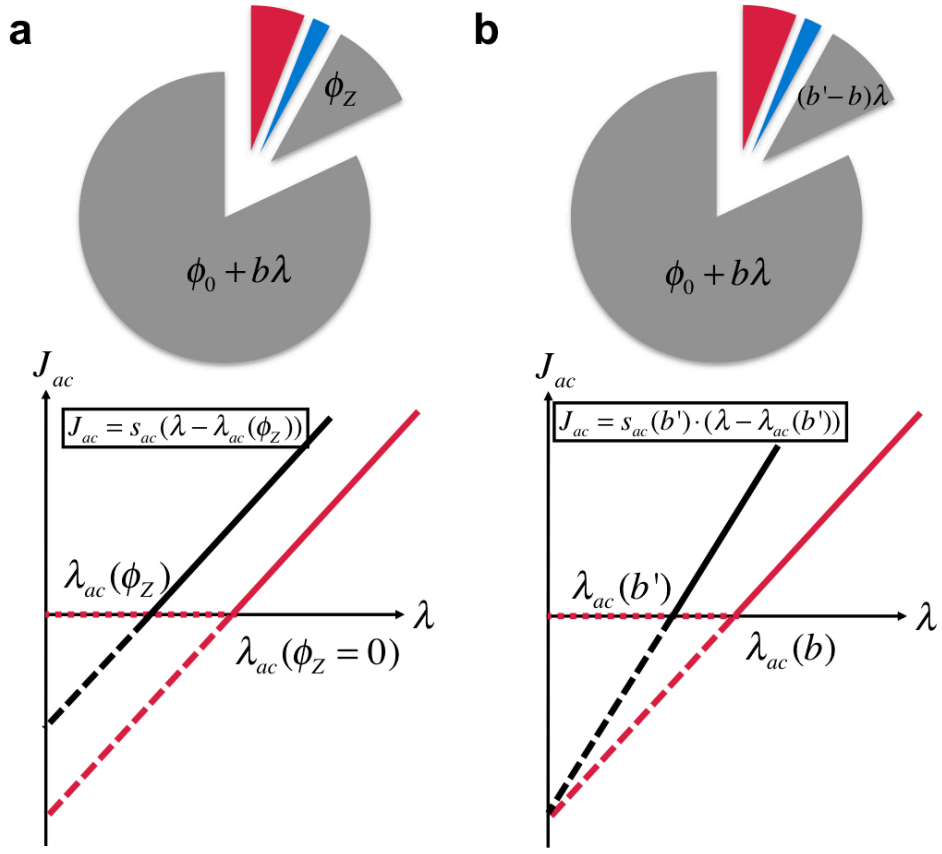

Figure N2: Illustration of model predictions for proteome limitation. Red and blue wedges represent the proteome fractions of fermentation and respiration pathway, respectively. **a,** For a constant level of protein overexpression (small gray wedge), the model predicts a shift of the acetate line to higher excretion rates (i.e., smaller λ_{ac}), but with an identical slope (see Eq. [S30]), as indicated by the black

line. This prediction is in good agreement with experimental data (see Figure 3a in the main text). **b**, Chloramphenicol leads to a lower efficiency of the ribosomal machinery, effectively increasing the parameter b to a higher value of b'. Hence, to sustain a certain growth rate, the bacterium needs to allocate a larger protein fraction to ribosomes. For a constant concentration of chloramphenicol, the size of this increase is proportional to growth rate (small gray wedge). The effect of chloramphenicol is therefore very similar to the effect of protein overexpression, only that the size of the additional proteome sector is proportional to growth rate. In this case, the model predicts a shift of the acetate line with an increased slope, but with an identical intercept for vanishing growth rates (see Eq. [S14]), as indicated by the black line. The experimental data is well described by this model prediction as shown in Figure 3c in the main text.

C3. Energy Limitation

The final class of perturbations directly interferes with the energy expenditure of the cell. Energy limitation can be accomplished, e.g., by dissipating membrane potential. This creates an additional (wasteful) component of the energy flux, w, such that the total energy usage of the cell becomes $J_E = \sigma\lambda + w$. The balance of energy flux Eq. [S*3*] thus becomes

$$J_{E,f} + J_{E,r} = \sigma\lambda + w\,, \qquad \text{[S31]}$$

Now solving the system defined by Eqs. [S*7*], [S*11*], and [S*31*], the growth rate dependence of acetate excretion rate for varying carbon uptake becomes

$$J_{ac} = S_{ac}\frac{\varepsilon_f}{e_f}\frac{\left(\sigma/\varepsilon_r + b\right)\lambda - \phi_{E,\max} + w/\varepsilon_r}{\varepsilon_f/\varepsilon_r - 1}\,. \qquad \text{[S32]}$$

The model predicts the acetate line to be shifted to slower growth rates with an identical slope, as illustrated in Figure N3a. This prediction is in excellent agreement with our experimental results using a leaky LacY mutant for energy dissipation (see Figure 3d of the main text).

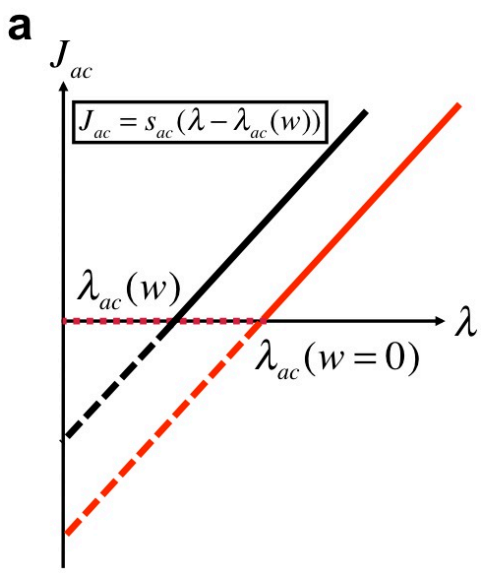

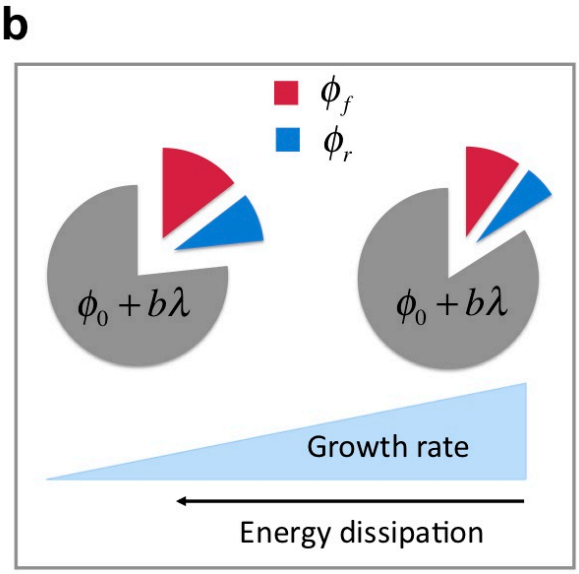

Figure N3: Illustration of model prediction for energy dissipation. a. The model predicts that energy dissipation leads to a parallel shift of the acetate line to higher acetate excretion rates, or lower intercept λ_{ac}, as indicated by the black line (see Eq. [S32]). **b.** Both energy sectors increase under this perturbation with decreasing growth rate (see Eqs. [S34], [S35] and Extended Data Table 2). Experimental data for acetate excretion under energy dissipation is presented in Figure 3d of the main text. The change in gene expression determined from mass spectrometry under energy dissipation buttresses this picture (see Extended Data Figs., 6 and 7).

At a fixed carbon uptake rate (e.g., at a fixed induction level for the titratable carbon uptake system in our experiment), we can solve the model (defined by Eqs. [S*7*], [S*11*], and [S*31*]) to obtain the change in proteome fractions by energy dissipation. This is done by taking derivatives of both sides of Eqs. [S*7*], [S*11*], and [S*31*] with respect to *w* and solving for $\frac{d}{dw}J_{E,f}$, $\frac{d}{dw}J_{E,r}$, and $\frac{d}{dw}\lambda$, while setting $\frac{d}{dw}J_{C,in}$ to zero. Since the dependences of these variables on *w* are linear, it is convenient to express the solutions in terms of $\Delta J_{E,f} \equiv w\cdot\frac{d}{dw}J_{E,f}$, $\Delta J_{E,r} \equiv w\cdot\frac{d}{dw}J_{E,r}$, $\Delta\lambda \equiv w\cdot\frac{d}{dw}\lambda$, with the results:

$$\Delta\lambda = -\frac{w\cdot\left(\frac{\varepsilon_f}{e_f}-\frac{\varepsilon_r}{e_r}\right)}{\beta\cdot\left(\varepsilon_f-\varepsilon_r\right)+\sigma\cdot\left(\frac{\varepsilon_f}{e_f}-\frac{\varepsilon_r}{e_r}\right)+b\cdot\varepsilon_f\cdot\varepsilon_r\cdot\left(\frac{1}{e_f}-\frac{1}{e_r}\right)}, \qquad [S33]$$

$$\Delta J_{E,f} = \frac{w\cdot\varepsilon_f\cdot\left(\beta-\frac{\varepsilon_r}{e_r}b\right)}{\beta\cdot\left(\varepsilon_f-\varepsilon_r\right)+\sigma\cdot\left(\frac{\varepsilon_f}{e_f}-\frac{\varepsilon_r}{e_r}\right)+b\cdot\varepsilon_f\cdot\varepsilon_r\cdot\left(\frac{1}{e_f}-\frac{1}{e_r}\right)}, \qquad [S34]$$

$$\Delta J_{E,r} = \frac{w\cdot\varepsilon_r\cdot\left(\frac{\varepsilon_f}{e_f}b-\beta\right)}{\beta\cdot\left(\varepsilon_f-\varepsilon_r\right)+\sigma\cdot\left(\frac{\varepsilon_f}{e_f}-\frac{\varepsilon_r}{e_r}\right)+b\cdot\varepsilon_f\cdot\varepsilon_r\cdot\left(\frac{1}{e_f}-\frac{1}{e_r}\right)}. \qquad [S35]$$

Using the model parameters presented in Extended Data Table 2 (worked out in Sec. D of this Note), we see that all quantities in the parenthesis of the above equations are positive. The model thus predicts that while energy dissipation reduces the growth rate, at the same time it increases the energy fluxes and hence the proteome allocation to both the fermentation and respiratory pathways – as a cellular response to reduction in energy biogenesis. This is best seen by expressing $\Delta\phi_f$ and $\Delta\phi_r$ in term of $\Delta\lambda$:

$$\Delta\phi_f = -\frac{\beta - \frac{\varepsilon_r}{e_r} b}{\frac{\varepsilon_f}{e_f} - \frac{\varepsilon_r}{e_r}} \Delta\lambda \,, \qquad \text{[S36]}$$

$$\Delta\phi_r = -\frac{\frac{\varepsilon_f}{e_f} b - \beta}{\frac{\varepsilon_f}{e_f} - \frac{\varepsilon_r}{e_r}} \Delta\lambda \,. \qquad \text{[S37]}$$

It is interesting to contrast the predicted responses to energy and proteome limitations: While a fixed degree of either perturbation leads to a parallel shift of the acetate line (Eqs. [S*30*] and [S*32*], respectively), varying proteome limitation gives rise to a linear decrease in the abundances of the energy sectors (Eqs. [S*23*], [S*24*]) while varying energy limitation gives rise to a linear increase in the abundances of the energy sectors (Eqs. [S*34*], [S*35*]). This contrast of behaviors is vividly seen in the relative changes in the levels of glycolytic and TCA enzymes obtained from mass spectrometry (Extended Data Figures. 6 and 7) in response to useless protein expression (orange) and energy dissipation (blue).

D. Parameter Determination

Eqs. [S*15*], [S*16*], [S*18*], [S*19*] give the key phenomenological parameters such as the threshold growth rate λ_{ac} in terms of the parameters of the model introduced in Sec. A (Eqs. [S*3*], [S*7*], [S*11*]). In order to make the model quantitatively predictive, it is necessary to determine the model parameters independently. Here we provide a detailed description of the procedure used to estimate these parameters. A summary of the parameter values is given in Extended Data Table 2.

D1. Carbon efficiencies (e_f and e_r in Eq. [S*11*]**):** For the conversion of NADH, NADPH and $FADH_2$ to ATP, we use the mean values of the range for an upper bound determined by Unden et al[11] and set ATP:NADH=2:1, ATP:NADPH=2:1 and ATP:$FADH_2$=1.15:1. The results of the main text and of the supplementary material are based on these conversion ratios, which yield satisfactory agreement with experimental data. Given these conversion ratios, the carbon efficiencies of fermentation and respiration, e_f and e_r respectively, defined by [S*10*], directly follow from the pathways in Extended Data Figure 2 with the results[6] $e_f = 2$ and $e_r = 4.4$.

[6] From the diagrams in Extended Data Figure 2, the above conversion ratios from NADH, NADPH, and $FADH_2$ gives ~12 ATP per glucose for the fermentation pathway and ~26 ATP per glucose for the respiration pathway. Converting these numbers to per carbon atom (which is the unit of the carbon flux used), we obtain the quoted values of e_f and e_r.

However, our key results are independent of the precise values of these conversion ratios as will be discussed below.

D2. Carbon demand for biomass synthesis (β in Eq. [S*11*]): β is defined by [S*9*] as the ratio between the carbon flux going to biosynthesis ($J_{C,BM}$) and the growth rate. For the four bioreactor cultures with various levels of lactose uptake titration, the values of $J_{C,BM}$ together with growth rates were determined (Extended Data Figure 3ab). Since the definition of β as given by [S*9*] holds for all growth range, to more accurately determine its value, we have carried out the CO_2, acetate, and carbon uptake measurements for another four conditions of more severe carbon limitation using the Pu-lacY strain (NQ381) grown in the bioreactor setup. The corresponding values of $J_{C,BM}$ were obtained following the same procedure in Extended Data Figure 3ab. β is the simply given as the slope of the line fitting the plot of $J_{C,BM}$ versus growth rate (Figure N4), i.e., $\beta \approx 28.5\,\mathrm{mM/OD_{600}}$.

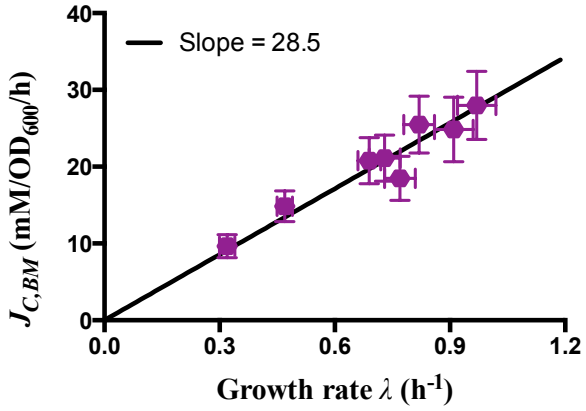

Figure N4: Estimate of β. The carbon flux going to biosynthesis $J_{C,BM}$ is plotted against the growth rate for the bioreactor cultures with various degrees of carbon uptake titration. The error bars of $J_{C,BM}$ indicate the propagated errors from the measurements and estimates of various fluxes. The error on growth rate is assumed to be 5%.

D3. Energy demand (σ in Eq. [S*3*]): We approximate energy demand as being proportional to growth rate with the proportionality σ. Under carbon limitation, the growth rate range with acetate excretion is small and therefore the total energy demand shows little variation. To probe the growth-rate dependene of energy demand for slower growth, we have carried out the CO_2, acetate, and carbon uptake measurements for more severe carbon limitation using the Pu-lacY strain (NQ381) grown in the bioreactor setup. The results demonstrate that energy production in *E. coli* is well described by a direct proportionality to growth rate, in accordance with previous studies[12]. In addition, the direct proportionalities of acetate excretion rate with growth rate found for increasing LacZ overexpression (discussed in Sec. C2 of this Note) indicate that the total energy demand is directly proportional to growth rate, i.e., $J_E = \sigma \cdot \lambda$.

Equating the energy flux J_E to J_{ATP}, σ was obtained using the J_{ATP} data for the titrations of lactose uptake (Extended Data Figure 3ab), i.e., $\sigma \approx 45.7\,\mathrm{mM/OD_{600}}$.

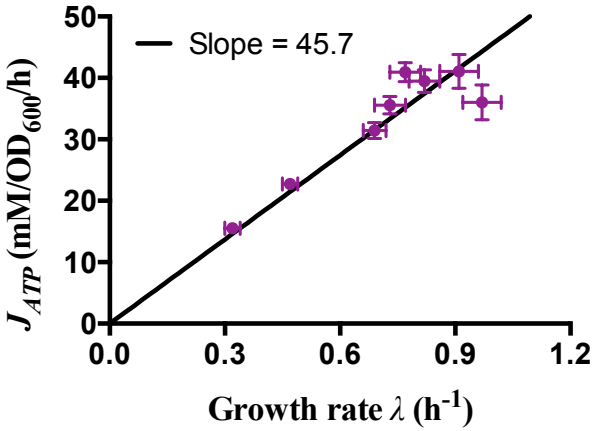

Figure N5: Estimate of σ. The value of σ is equal to the slope of the origin-passing line fitting the total ATP flux J_{ATP} versus growth rate in bioreactor. The data are shown in Extended Data Figure 3b. The error bars on the ATP flux were results of propagated errors from underlying measurements and estimates. An error of 5% on growth rate measurement was assumed.

D4. Proteome fractions (b and $\phi_{E,\max}$ in Eq. [S7]): Protein cost plays a central role in our model and therefore the measurement of several model parameters requires protein quantification. Again for the bioreactor carbon limitation series, we determined the size of the fermentation and respiration proteome fractions (i.e., ϕ_f and ϕ_r), using mass spectrometry in combination with flux balance analysis. See Supplementary Note 3 for the detailed description of the estimates. By fitting the total energy production sector ($\phi_f + \phi_r$) with a linear function, we determined the parameters $\phi_{E,\max}$ and b appearing in Eq. [S7] (Figure N6), i.e., $\phi_{E,\max} \approx 0.19$ and $b \approx 0.12$.

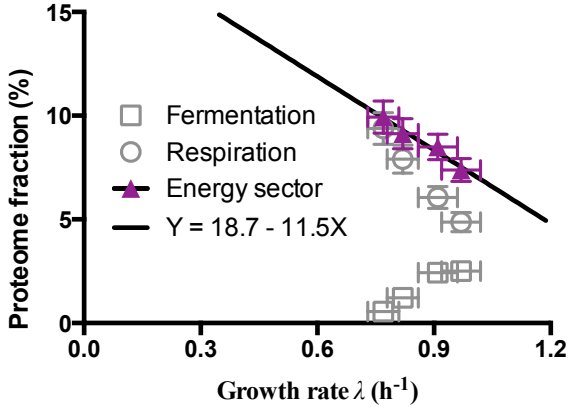

Figure N6: Proteome fractions of energy production pathways. Proteome fractions of the fermentation pathway (ϕ_f, gray squares), the respiration pathway (ϕ_r, gray circles) as well as the total energy sector ($\phi_f + \phi_r$, purple triangles) determined by Mass Spectrometry and flux analysis are plotted as a function of growth rate in bioreactor. The growth rate dependence of the total energy sector was fitted by a linear function, which was used to determine the model parameters $\phi_{E,\max}$ and b.

D5. Proteome efficiencies (ε_f and ε_r in Eq. [S7]): The proteome efficiencies are defined by [S6] as the ratios of energy fluxes to proteome fractions. Since we have both the proteome fractions (ϕ_f and ϕ_r) and energy fluxes ($J_{ATP,f}$ and $J_{ATP,r}$) for the two pathways in the bioreactor carbon limitation series (Extended Data Figure 3b), the proteome efficiencies ε_f and ε_r can be obtained as slopes of lines fitting respective energy flux versus proteome fraction (Figure N7).

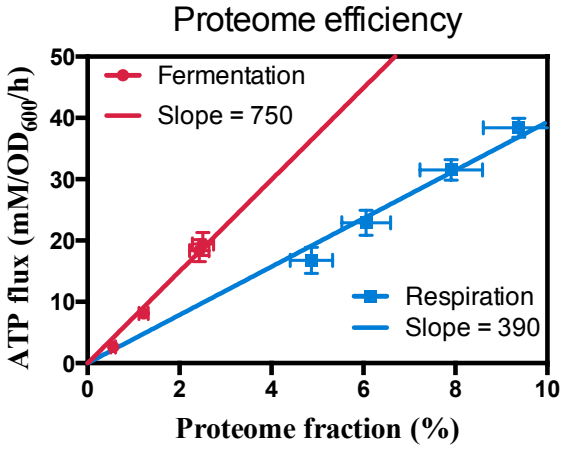

Figure N7: Protein efficiencies of energy production pathways. For the lactose titration series, the proteome fractions and ATP fluxes of the two pathways were obtained for 4 different bioreactor growth conditions (See Supplementary Notes 2 and 3). The value of the protein efficiency of a pathway is equal to the slope of the origin-passing line that fits the ATP flux versus proteome fraction of the pathway.

D6. Consistency of the parameters: As illustrated in Extended Data Figure 3cd, using the set of parameters determined above (summarized in Extended Data Table 2), the model solution (Eqs. [S14], [S17]) satisfactorily describes the experimental data obtained for acetate excretion (J_{ac}) and respiratory CO_2 evolution ($J_{CO_2,r}$) in the bioreactor carbon limitation series, demonstrating the consistency of the parameters.

Supplementary Note 2: Estimate of respiration flux

Introduction

The model described in Supplementary Note 1 makes detailed predictions on the metabolic fluxes through the two energy pathways for different strains and conditions. While the metabolic flux through the fermentation pathway is directly proportional to the acetate excretion rate, it is not as straightforward to obtain the flux through the respiration pathway. Here we describe the procedures for obtaining the flux through the respiration pathway.

Flux balance

The carbon flux through respiration ($J_{C,r}$) can be deduced using carbon balance, as shown in Eq. [S*8*]: The total carbon influx ($J_{C,in}$) is equal to the sum of three carbon fluxes, the carbon flux through fermentation ($J_{C,f}$), the carbon flux going to biomass production ($J_{C,BM}$), and $J_{C,r}$. (For convenience, we use the term 'carbon flux' to refer to the flux of *single* carbon atoms. For example, for one unit of glucose influx, $J_{C,f}$ is equal to 6 because one glucose molecule contains 6 carbon atoms.) $J_{C,f}$ is given by the acetate flux (J_{ac}) as $J_{C,f} = 3 \cdot J_{ac}$. Using the equation $J_{C,BM}(\lambda) = \beta\lambda$, $J_{C,BM}$ is readily obtained by just measuring the growth rate λ, with the value of β determined in Sec. D of Supplementary Note 1. Since $J_{C,in}$ can be directly measured, $J_{C,r}$ can be in principle be calculated according to Eq. [S*8*]. In practice, however, $J_{C,r}$ obtained in this way would have large uncertainty – because $J_{C,BM}$ is much larger than $J_{C,r}$, a small relative uncertainty in $J_{C,BM}$ would translate into a huge relative uncertainty in $J_{C,r}$.

To avoid this problem, we turn to the flux balance equation for CO_2,

$$J_{CO2,f} + J_{CO2,r} + J_{CO2,BM} = J_{CO2}\,, \qquad \text{[S38]}$$

where $J_{CO2,f}$, $J_{CO2,r}$, and $J_{CO2,BM}$ refer to the CO_2 fluxes produced by the fermentation, respiration, and biomass production, respectively, and J_{CO2} is the total CO_2 production rate by the cell. As we will show below, the CO_2 fluxes by the three pathways have similar magnitude and therefore noises in measurements or estimates of $J_{CO2,f}$, $J_{CO2,BM}$, and J_{CO2} do not result in magnified noise in the estimate of $J_{C,r}$.

Measurement of total CO_2 production rate

To measure the CO_2 production rate, we use a bioreactor setup. The system has an air-inlet and an outlet for exhaust gas. A constant flow (f) of air (containing a CO_2 concentration of c_0) to the inlet is maintained by a mass flow controller. The exhaust gas line is connected to a CO_2 sensor and the concentration of CO_2 at time t, $c(t)$, in the exhaust gas is constantly measured. The OD_{600} of the bacterial culture (with volume V) is measured between every half-doubling time and one doubling time and the OD_{600} at the time t, $OD(t)$, can be deduced from the growth curve. At steady state, the CO_2 production rate is equal to the CO_2 flow, or

$$OD(t) \cdot V \cdot J_{CO2} = k \cdot f \cdot (c(t) - c_0)\,, \qquad \text{[S39]}$$

where $k = 39.3$ μmol/ml is a constant converting gas volume and amount of gas under the condition of 1 atm and 37°C. Re-arranging Eq. [S*39*] gives

$$c(t) = J_{CO2} \cdot \frac{V}{k \cdot f} \cdot OD(t) + c_0\,. \qquad \text{[S40]}$$

The slope (s) of the $c(t)$ versus $OD(t)$ plot can be obtained by fitting the data with a line (Figure N8). Subsequently, J_{CO2} is given by

$$J_{CO2} = \frac{k \cdot f}{V} \cdot s \,. \qquad [S41]$$

Using a culture of NCM3722 grown on lactose minimal medium as an example, where f = 400 ml/min, V = 410 ml, and s = 0.0046 OD^{-1}, we have J_{CO2} = 10.57 mM/OD/h.

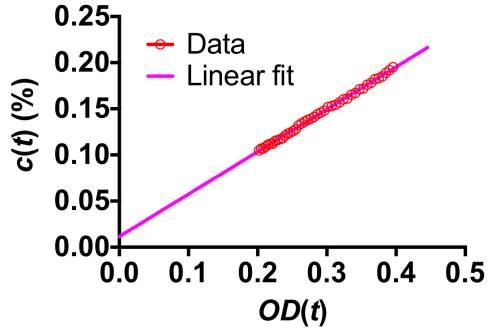

Figure N8: CO_2 concentration versus OD_{600}. The concentration (%) of CO_2 in the bioreactor exhaust gas is plotted a function of the OD_{600} of the cell culture.

CO_2 production associated with biomass production

We assume that

$$J_{CO2,BM} = \lambda \cdot \beta_{CO2} \,, \qquad [S42]$$

where β_{CO2} (in unit of mmol/g) represents the amount of CO_2 produced as the by product of biosynthetic reactions needed to make 1 g of cell dry weight (not including the energy and reduction power that need to be generated to perform biosynthesis). We want to estimate the value of β_{CO2} for our strain, so that $J_{CO2,BM}$ can be obtained for each growth rate corresponding to each growth condition. We will obtain this value using data available in the literature, and then follow up with some cross checks.

In cases where $J_{CO2,f}$ and $J_{CO2,r}$ can be deduced from determined flux distribution, we can use Eq. [S*38*] to get $J_{CO2,BM}$ provided that J_{CO2} has also been measured. Further given the growth rate λ, we can obtain β_{CO2} from Eq. [S*42*]. In Fischer et al[4], we find $J_{CO2,f}$ = 7.2 mmol/g/hr, $J_{CO2,r}$ = 6.3 mmol/g/hr, and J_{CO2} = 19.6 mmol/g/hr for growth of *E. coli* MG1655 cells in glucose minimal medium. This gives $J_{CO2,BM}$ = 6.1 mmol/g/hr based on Eq. [S*38*], which leads to β_{CO2} = 7.18 mmol/g given the observed growth rate of λ = 0.85 /hr (based on Eq. [S*42*]).

Next we estimate the value of β_{CO2} using flux analysis. We start from the known biomass composition and deduce from biochemical stoichiometry the amount of CO_2 involved for making each of the biomass constituent. Using the latest *E. coli* reconstruction model iAF1260[13], we ran a Flux Balance Analysis (FBA) to maximize biomass production rate under the constraint of limited glucose uptake rate. From the resulting CO_2 production flux, we obtained β_{CO2} = 6.32

mmol/g. This number is the theoretical minimum for a given biomass composition, because by maximizing biomass production rate FBA automatically minimizes the production of other carbon fluxes (e.g., CO_2 flux, acetate flux, etc). In reality, the biomass composition, in particular, the RNA/protein ratio, is dependent on the growth rate. To see how sensitive this number depends on biomass composition, we vary the biomass composition to see how the value of β_{CO2} changes accordingly.

In the original iAF1260 model, protein and RNA account for about 56% and 21% of the dry weight, respectively, while the remaining 23% includes about 9% lipid, 2.5% murein, 3% DNA, 2.5% glycogen, 3% outer membrane materials, and 3% soluble metabolites[13]. Assuming this remaining 23% is growth-rate independent, we vary the mass fraction of protein from 40% to 70% (with the corresponding variation of RNA mass fraction from 37% to 7%). See Figure N9a for the corresponding values of β_{CO2}.

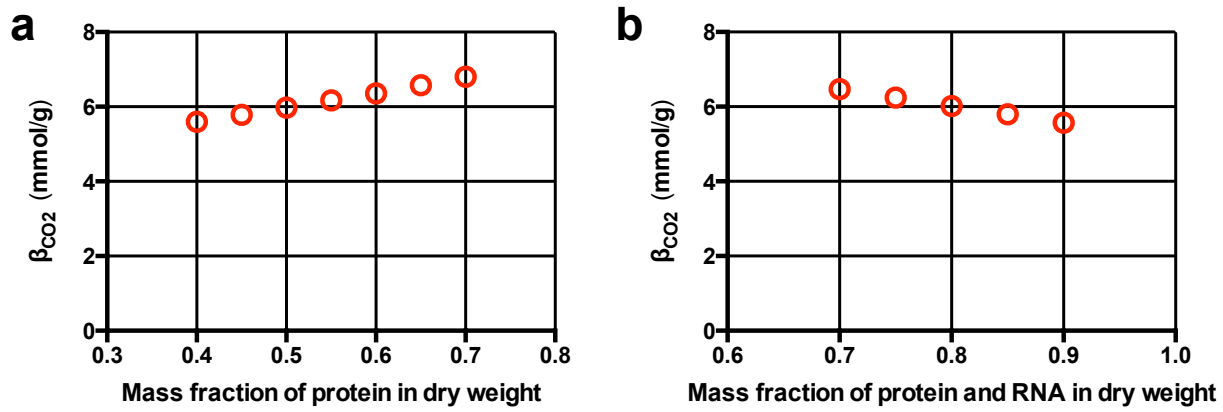

Figure N9: Dependence of the value of β_{CO2} on biomass composition. a. β_{CO2} as a function of mass fraction of protein. **b.** β_{CO2} as a function of mass fraction of protein and RNA.

Since the total protein fraction can change as well for different strains, we also varied the total mass fraction of protein and RNA, from 70% to 90%, assuming the relative composition of the rest mass fraction is fixed at 23%. See Figure N9b for the corresponding values of β_{CO2}.

The results above show that β_{CO2} does not have strong dependence on biomass composition, with ~10% variation even for the extreme biomass compositions. Since the above values obtained from yield-maximizing FBA calculations constitute a theoretical minimum (for each biomass composition), we conclude that the first estimate obtained from the experimental data of Fischer et al[4], i.e., $\beta_{CO2} \approx 7.2$ is a reasonable estimate of this parameter, with an uncertainty of ~10%.

CO_2 flux by respiration

Now with β_{CO2} determined, $J_{CO2,BM}$ can be determined from Eq. [S*42*] simply by measuring growth rates. And $J_{CO2,f}$ is related to the acetate flux J_{ac} with chemical stoichiometry (which is 1 because the net chemical reaction for fermentation is 6Glucose → 2Acetate + 2CO_2), i.e., $J_{CO2,f} = J_{ac}$. We then have from Eq. [S*38*]

$$J_{CO2,r} = J_{CO2} - J_{ac} - \beta_{CO2} \cdot \lambda \,. \qquad \text{[S43]}$$

For the bioreactor carbon limitation series, we have measured the total CO_2 production rate (J_{CO2}), acetate excretion rate (J_{ac}), and growth rate (λ), so that Eq. [S*43*] can be used to compute $J_{CO2,r}$. The values of both the measured and deduced fluxes for the bioreactor series are shown in Extended Data Figure 3.

Supplementary Note 3: Estimate of the abundance of proteins in energy biogenesis

Introduction

As demonstrated in the main text, the proteome efficiencies of the energy pathways (i.e., ε_f, ε_r) are crucial parameters in our approach to understanding the acetate overflow problem. To experimentally determine their values, we need to estimate the abundances of proteins devoted to each of the energy biogenesis pathways. Since many reactions in central metabolism provide flux for both biosynthesis and energy biogenesis, we need to not only estimate the absolute abundance of each protein, but also determine for each reaction what fraction of the flux is devoted to each of the two energy biogenesis pathways. In this note, we describe our approach for achieving these goals.

A. Absolute protein abundance quantitation using mass spectrometry

Protein mass spectrometry generates accurate and precise data on relative protein abundances[3]. To infer absolute protein abundances from relative protein abundances, we need a standard for which the absolute protein abundances are known. Recent work shows that the method of "ribosome profiling" can reliably quantify absolute protein abundance for exponentially growing *E. coli* cells[14]. We will thus use the absolute protein abundances estimated from this reference as the standard.

Our specific goal is to quantify the absolute abundance of each protein involved in energy biogenesis for the bioreactor carbon limitation series, with various titrations of lactose uptake (Extended Data Figure 3). What we did was first to use mass spectrometer to obtain the relative protein abundance for the four samples in the series together with one sample of EQ353 grown in glucose minimal medium. (See the section on Proteomic mass spectrometry in the Methods for details of the mass spectrometry procedure.) The strain EQ353 grown in the same glucose minimal medium was used for the ribosome profiling study of Li et al[14]. Using the estimates of the absolute abundances of proteins of EQ353 obtained in this reference, we are able to estimate the absolute abundances of many proteins in our bioreactor carbon limitation series. The results are listed in Table N1 for proteins involved in energy biogenesis, including enzymes involved in the uptake and breadown of lactose, enzymes of glycolysis and TCA, and those involved in oxidative phosphorylation and proton-driven ATPase.

As shown in Table N1, only 34 (out of 74 proteins listed) have relative abundance assignment for both the carbon limitation series and EQ353. The missing assignments are due mostly to a limited coverage by mass spectrometer. This limited protein coverage, however, does not prevent us from obtaining meaningful estimates for the total abundances of proteins in energy biogenesis pathways, because mass spectrometer detects the abundant proteins well: For EQ353 grown in glucose minimal medium, the 34 proteins comprise 88% of the abundance of all proteins in the table (as determined by ribosome profiling). Furthermore, among the rest of proteins in the list, 15 are subunits of protein complexes which contain one or more subunits with relative abundance assignment. Their abundances can be obtained by assuming their relative abundance is the same as the relative abundance of other subunits in the same protein complex. For example, among the three subunits of F_0 complex of ATP synthase, only AtpF has relative abundance assignment; the other two subunits, AtpB and AtpE, are assumed to have the same

relative abundance. Together, the 49 proteins comprise 93% of the abundance of all proteins in the table for EQ353 grown in glucose minimal medium. We expect most of these proteins to be similarly abundant in NQ381 under the growth conditions of interest. Important exceptions are 8 enzymes specific to lactose utilization (as compared to glucose utilization), i.e., LacZ, LacY, Glk, Pgm, GalM, GalK, GalT, and GalE, which are hardly expressed in EQ353 (grown in glucose), but should be abundantly expressed in NQ381 strains in condition of our interest (grown in lactose). To obtain accurate estimates for LacZ levels, we assayed the β-galactosidase activity for one of the conditions in the carbon limitation series, NCM3722 cells grown in lactose minimal medium. With a Miller Unit (using a non-plate reader protocol) of 4700 and a conversion factor of 1.7% proteome fraction for 10,000 MU^2, we obtained a proteome fraction of 0.78% for the abundance of LacZ from this strain in this condition. This was used to fix the abundance of LacZ for the other conditions of the carbon limitation series. (given the relative protein abundances listed in Table N1). The estimated absolute abundances of the 50 proteins for the carbon limitation series are shown in Table N1.

Table N1: Absolute abundance of proteins in energy biogenesis determined by mass spectrometry with standard. Table is available as an appendix at the end of this SI. Column B lists the gene names for the 74 proteins that are involved in energy biogenesis for cells grown in lactose minimal medium (The gene name 'lpdA' is listed twice because it functions as a subunit for both the pyruvate dehydrogenase and 2-oxoglutarate complex.). Column A lists the pathway or the protein complex for the corresponding proteins. Columns C-G are for 'Relative abundance' as determined by the mass spectrometry. Note that not all entries have data due to limited coverage. Column H lists the absolute abundance for the strain EQ353 grown in glucose minimal medium, as determined in Li et al[14] by ribosomal profiling method. In Columns I-L, the absolute abundances in the four samples of the carbon limitation series are listed for 50 proteins: 34 were determined from the relative abundance data (Columns C-G) together with the standard absolute abundance data (Column H); 15 (as indicated in corresponding entries in Column M) were determined in same way but using the relative abundance data for subunits in the same protein complex; One protein (LacZ) was determined by using both the relative abundance data and LacZ assay (as indicated in Column M).

For the remaining 24 proteins missing absolute abundance assignment from the above procedure, we used spectral counting data by mass spectrometry to estimate their abundances (see the Proteomic mass spectrometry section in the Methods) except for LacY, which is a membrane protein and is poorly detected by the mass spectrometry method used. While the method of spectral counting is a crude way for estimating absolute abundance for individual proteins[15], the resulting uncertainties associated with the 23 absolute protein abundances do not have significant effect on later estimate of proteome efficiencies because the sum of these abundances accounts for only a few percent of the total mass of all listed proteins. In Table N2, we list the spectral counting data for the 23 proteins (and for the other 51 proteins for completeness). Finally, to estimate the abundance of LacY, we turned to enzyme kinetics by using the measured lactose uptake rate (Extended Data Figure 3) and a lower bound value[7] of turnover rate of 20 sec^{-1} for the permease[16].

[7] The turnover rate of the lactose permease ranges from 20 to 50 sec^{-1} according to the reference. Using a lower bound value of the turnover rate reduces the possibility of underestimating the LacY protein abundance. An overestimate will decrease the difference between the two proteome efficiencies.

Table N2: Absolute abundance of proteins in energy biogenesis determined from mass spectrometry spectral counting data. Table is available as an appendix at the end of this SI. Column B lists the gene names for the 74 proteins that are involved in energy biogenesis for cells grown in lactose minimal medium (The gene name '*lpdA*' is listed twice because it functions as a subunit for both the pyruvate dehydrogenase and 2-oxoglutarate complex.). Column A lists the pathway or the protein complex for the corresponding proteins. Columns C-G list the spectral counting data for 23 of the 24 proteins that have no assigned values in Table N1 (excluding LacY). Columns H-L list the spectral counting data for the 50 proteins that have assigned values Table N1.

The results of the LacY abundance together with the abundances estimated from the two procedures above are merged into one table, Table N3.

Table N3: Summary table for the absolute abundance of all proteins in energy biogenesis. Table is available as an appendix at the end of this SI. Column B lists the gene names for the 74 proteins that are involved in energy biogenesis for cells grown in lactose minimal medium (The gene name 'lpdA' is listed twice because it functions as a subunit for both the pyruvate dehydrogenase and 2-oxoglutarate complex.). Column A lists the pathway or the protein complex for the corresponding proteins. Columns C-F list the absolute abundances for the 74 proteins, with 50 given in Table N1 and 23 in Table N2, Column G indicates those proteins whose abundance are based on spectral counting data, and denotes the special method for obtaining the LacY abundance.

B. Partitioning the mass of individual proteins based on fluxes

Most of the proteins in Table N3 produce fluxes that go into the two energy biogenesis pathways and the biomass synthesis pathways. To determine the protein masses devoted to each pathway, we simply partition the mass in proportion to the flux directed to each pathway. Consider for example a protein p whose abundance is a fraction ϕ_p of the proteome. If the total carbon flux it carries (J_p) is composed of the fermentation flux ($J_{p,f}$), respiration flux ($J_{p,r}$), and biomass flux ($J_{p,BM}$), with $J_p = J_{p,f} + J_{p,r} + J_{p,BM}$, then protein p contributes

$$\phi_{p,i} = \phi_p \cdot \frac{J_{p,i}}{J_p} \qquad \text{[S44]}$$

to the pathway i (i.e., $i = f$ for fermentation pathway, $i = r$ for respiration pathway, and $i = BM$ for biomass synthesis pathway).
The total proteome fraction for the pathway i is then simply

$$\phi_i = \sum\nolimits_p \phi_{p,i} \qquad \text{[S45]}$$

While ϕ_p has been determined in Sec. A of this note (see Table N3 for the value of each protein), we need to obtain values of $J_{p,i}$ in order to carry out the partition of ϕ_p among the pathways using Eq. [S*44*]. Within each of the energy biogenesis pathways or the biomass synthesis pathway, the stoichiometry between the fluxes of different proteins is fixed; see Table N4 for the values. Let us denote $S_{p,i}$ as the stoichiometry for protein p in pathway i. The flux for the protein is then given by

$$J_{p,i} = S_{p,i} \cdot J_{C,i}, \qquad \text{[S46]}$$

Where $J_{C,i}$ is the carbon flux feeding to the pathway i. See Table N4 for values of fluxes for the bioreactor carbon limitation series. The values of $\phi_{p,i}$ obtained from Eqs. [S*44*] and [S*46*] for the same series are also shown in Table N4.

Table N4: Partition of protein mass among the pathways. Table is available as an appendix at the end of this SI. Column B lists the gene names for the 74 proteins that are involved in energy biogenesis for cells grown in lactose minimal medium (The gene name 'lpdA' is listed twice because it functions as a subunit for both the pyruvate dehydrogenase and 2-oxoglutarate complex.). Column A lists the pathway or the protein complex for the corresponding proteins. Columns C-E list the stoichiometry for the three pathways. The stoichiometry for the biomass production pathway is based on Table 5 in Chapter 5 of Neidhardt et al7, where the amount of precursors needed to produce one unit of biomass is listed. To get the stoichiometry for the oxidative phosphorylation proteins, it was assumed that 1 NADPH = 2 ATP, 1 NADPH = 2 ATP, and 1 FADH2 = 1 ATP. However, the exact values of converting factors do not matter for the partition of protein mass among the pathways because it is the relative values of stoichiomery between the pathways for the same enzyme that determine the partition, i.e., Eqs. [S44] and [S46]. Columns F-L list for the condition of NQ381 with 400 μM 3MBA the protein abundances (Column F), fluxes (Columns G-I), and protein mass allocated to each of the three pathways (Columns J-L). The format of the data is similar for the other 3 growth conditions, i.e., NQ381 with 500 (Columns M-S) and 800 μM 3MBA (Columns T-Z), and WT NCM3722 in lactose minimal medium (Columns AA-AG).

The proteome fractions for the two energy pathways were then simply obtained by Eq. [S*45*], which are shown in Figure 4.

We also considered the possibility that the proteomic response to oxidative stress should be associated with energy biogenesis, since reactive oxygen species (ROS) is apparently related to oxygen utilization during energy biogenesis. This possibility was however ruled out by Seaver & Imlay[17], who found that the production of the hydrogen peroxide was not diminished by mutations that eliminated most repiratory functions. We therefore have not included the proteins involved in the oxidative response as part of energy biogenesis. Nevertheless, to examine its possible effect, we estimated the abundance of oxidative stress response proteins and found it to be about 1.8%, approximately constant across the bioreactor samples. Our main result, the relative proteome efficiency between fermentation and respiration pathway, is hardly affected by the inclusion of oxidative response since both fermentation and respiration pathways comprise of oxidative phosphorylation components and hence would both be taxed with the additional cost.

Supplementary Note 4: Alternative pathways in central metabolism

Introduction

In obtaining the parameters and predictions of the model, we have assumed a simple central metabolism, consisting of mainly the glycolysis pathway (or the EMP pathway) and the TCA cycle, as reflected by the simple illustration of the fermentation and respiration pathways in Extended Data Figure 2. However, there exist alternative pathways in central carbon metabolism, including the Entner-Doudoroff (ED) pathway, the pentose phosphate pathway, and the recently discovered PEP-glyoxylate cycle[4]. While the usage of the ED pathway by *E. coli* K-12 has been shown to be minimal[18,19], the other two alternative pathways can carry substantial metabolic flux in certain growth conditions. In Sec. A below, we demonstrate that the PEP-glyoxylate cycle, as an alternative pathway to the TCA cycle, does not play a significant role as compared to the latter in the growth conditions of this study, by finding much smaller effects on both acetate excretion and global gene expression from deleting genes in the PEP-glyoxylate cycle than in the TCA cycle. In Sec. B, we find that inclusion of the pentose phosphate pathway to central metabolism only has small effect on the results based on the simplified description of central metabolism. This is because the upper part of the glycolysis (to which the pentose phosphate pathway is an alternative) constitutes much smaller proteome fraction than the lower part of the glycolysis. A key result of our study, the predicted increase of the respration flux under carbon limitation, is essentially unaffected as illustrated in Figure N10 where 20% of the carbon uptake is assumed to go to the pentose phosphate pathway (denoted as $x = 20\%$ in the detailed analysis in Sec. B).

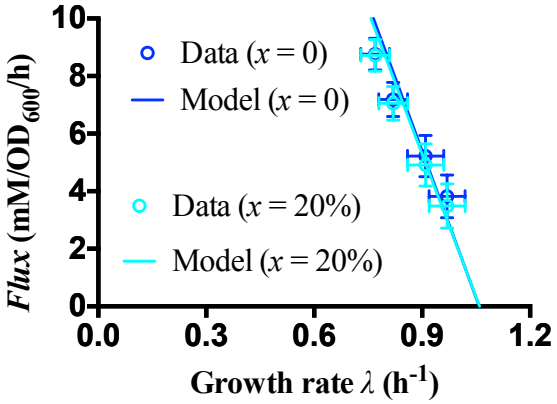

Figure N10: The estimated respiration CO_2 flux for $x = 20\%$ and the corresponding model description. For comparison, the case of $x = 0$ as shown in Extended Data Figure 3c is replotted here as blue symbols and lines.

A. The PEP-glyoxylate cycle

Recently it was discovered that the *E. coli* cell can oxidize carbohydrates via the novel PEP-glyoxylate cycle[4]. In the cycle, two P-enolpyruvate molecules are first converted into two acetyl-CoA molecules, which are then converted into one molecule of oxaloacetate using part of the TCA cycle and the glyoxylate shunt, and finally one PEP molecule is regenerated from the oxaloacetate molecule. The net reaction of the cycle is that one PEP molecule is oxidized into

three CO2 molecules, yielding energy molecules, which are biochemically similar to the TCA cycle but utilizing a different set of enzymes. Unique components of the PEP-glyoxylate cycle include the constituents of the glyoxylate shunt and PEP carboxykinase, which are not utilized when carbohydrate is oxidized via the TCA cycle.

To determine to what extent the cycle is functioning in our strain, we have measured acetate excretion for the *aceA* (encoding isocitrate lyase, which is part of the glyoxylate shunt) and *pckA* (encoding PEP carboxykinase) knockout strains grown in different carbon sources. As a control, we have also carried out the measurements for the *sucC* (encoding a subunit of succinyl-CoA synthetase, which is part of the TCA cycle) deletion strain. The results show essentially no effect on acetate excretion by the *aceA* and *pckA* knockouts, in contrast to the significant increase of acetate excretion by the *sucC* knockout (Figure N11). This suggests that the PEP-glyoxylate cycle works at a much lower degree than the TCA cycle in these growth conditions.

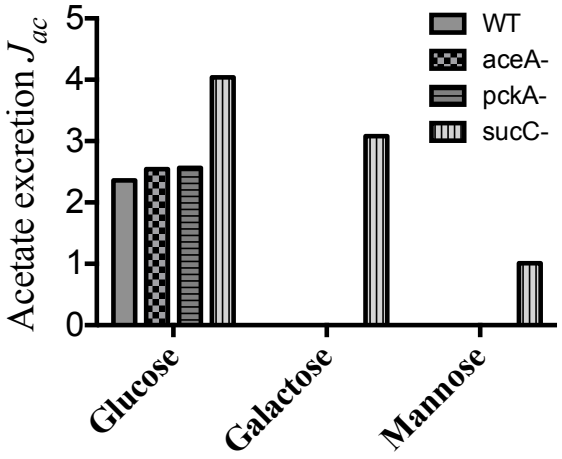

Figure N11: The effect of various gene knockouts on acetate excretion. The three knockout strains, *aceA*-, *pckA*-, and *sucC*- strains, together with the WT strain were grown on three different carbon sources.

To further investigate the role of the PEP-glyoxylate cycle, we have measured protein expression for the three knockouts relative to the WT strain using protein mass spectrometry. The effects of the *aceA* and *pckA* knockouts on protein expression are much smaller compared to that of the *sucC* knockout, as demonstrated by the highly peaked distributions of protein abundance around 1 (relative to WT) for the first two mutants (Figure N12).

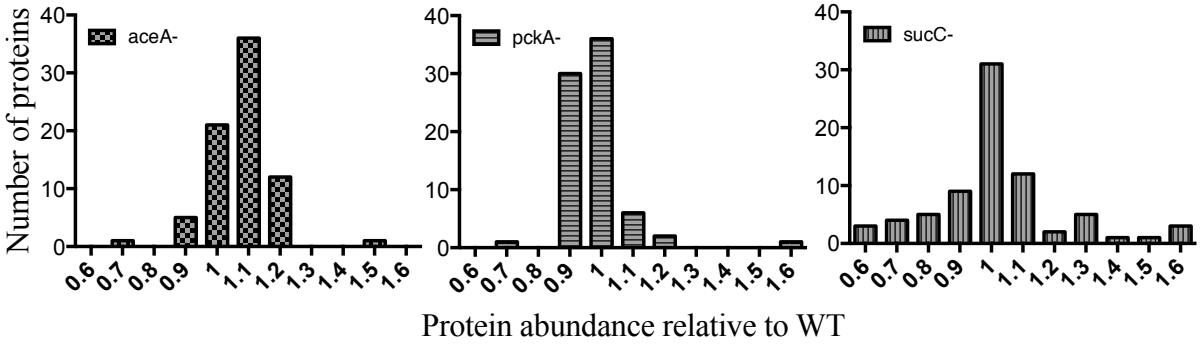

Figure N12: Distributions of relative protein abundances for the three gene knockouts. All three strains together with the WT strain were grown on the mannose minimal medium. X-axis of each of the three plots indicates the ratio of the protein abundance relative to that of the WT strain. A value of 1 means no change of protein abundance relative to WT. The histograms are for the top abundant proteins observed by mass spectrometry.

In summary, the acetate excretion and protein expression results suggest that compared to the TCA cycle, the alternative PEP-glyoxylate cycle does not play a significant role in the growth conditions in this study.

B. The pentose phosphate pathway

In addition to supplying some of the carbon precursors for biomass synthesis, the pentose phosphate pathway can function as an alternative pathway to the upper part of the glycolysis, by beginning with an glycolysis intermediate molecule, glucose-6-phosphate (G6P), passing two precursor metabolites, D-ribose-5-phosphate (R5P), and erythrose-4-phosphate (E4P), and ending with the formation of two other intermediates molecules of glycolysis, fructose-6-phospahte (F6P) and D-glyceraldehyde-3-phosphate (G3P), as illustrated in Figure N13.

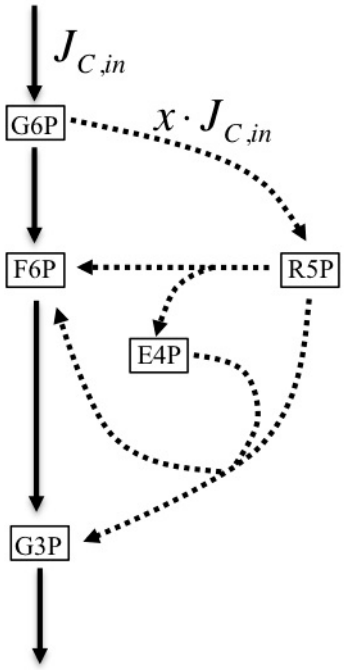

Figure N13: The pentose phosphate pathway can function as an alternative pathway to the upper part of the glycolysis. Dashed arrows indicate the biochemical reactions of the pentose phosphate pathway, and black arrows those of the glycolysis pathway. Only key metabolites are shown and arrows can represent multiple biochemical reactions between the metabolites shown.

Written with exact stoichiometry for major metabolites including CO_2 and the energy molecule NADPH in the pathway, the effective biochemical reaction is

$$\mathrm{G6P} \rightarrow \frac{2}{3}\mathrm{F6P} + \frac{1}{3}\mathrm{G3P} + \mathrm{CO_2} + \mathrm{NADPH}. \qquad [S47]$$

To investigate the effect of the pentose phosphate pathway, we denote the flux carried by the pathway as $x \cdot J_{C,in}$, where $J_{C,in}$ is the total carbon influx and x represents the fraction of the total flux that goes to the pathway. So far, we have assumed that $x = 0$ and the pathway (represented as Eq. [S*47*]) is not included in our definition of the fermentation and respiration pathways (Extended Data Figure 2). Flux measurements, however, show that x can be substantial, with x having a value of around 20% for growth on glucose minimal medium[18,19]. Here, by following the same procedures for estimating model parameters in Supplementary Notes 1-3, we determine the effect of the inclusion of the pentose phosphate pathway on the model parameters using the bioreactor data, i.e., the influence of various values of x on the parameters in Extended Data Table 2.

To carry out the estimates for model parameters, the first step is to define the fermentation and respiration pathways. To include the pentose phosphate pathway into the definitions, we assume that for either fermentation or respiration the fraction of the total influx going through the pentose phosphate pathway is also x. For example, for a total carbon influx through fermentation $J_{C,f}$, the fermentation flux that goes through the pentose phosphate pathway is $x \cdot J_{C,f}$. This is illustrated for fermentation and respiration in Figure N14.

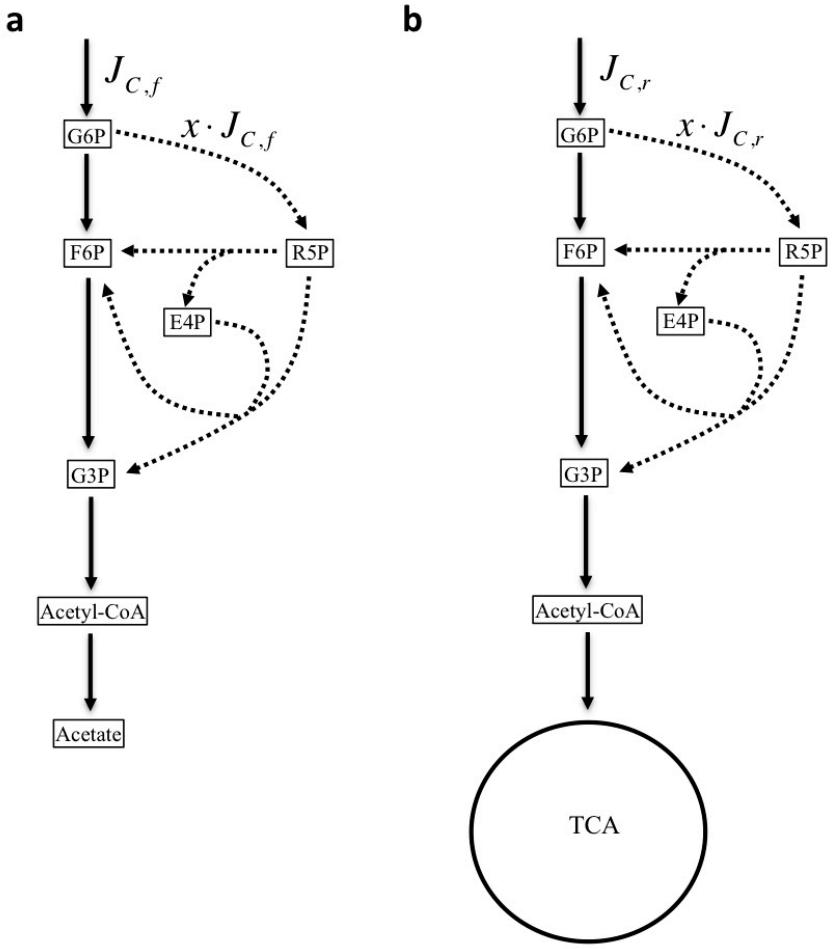

Figure N14: Modified fermentation and respiration pathways with the inclusion of the pentose phosphate pathway. Dashed arrows indicate the biochemical reactions of the pentose phosphate

pathway, and black arrows those of the glycolysis pathway and the TCA cycle. Only key metabolites are shown and arrows can represent multiple biochemical reactions between the metabolites shown.

For a given value of x, the biochemical stoichiometry for either fermentation or respiration pathways is fixed. Using glucose (GLC) as an example of an uptake carbon, for fermentation, the stoichiometry for carbon-containing metabolites and energy metabolites is

$$\begin{aligned} \mathrm{GLC} \rightarrow\ & (2-\tfrac{1}{3}x)\mathrm{ACE}+(2+\tfrac{2}{3}x)\mathrm{CO2} \\ & +(4-\tfrac{2}{3}x)\mathrm{ATP}+(4-\tfrac{2}{3}x)\mathrm{NADH}+(x)\mathrm{NADPH}, \end{aligned} \qquad [S48]$$

where ACE represents the metabolite acetate and numbers inside the parentheses indicate the stoichiometry. And for respiration, the stoichiometry is

$$\begin{aligned} \mathrm{GLC} \rightarrow\ & 6\ \mathrm{CO2}+(4-\tfrac{2}{3}x)\mathrm{ATP} \\ & +(8-\tfrac{4}{3}x)\ \mathrm{NADH}+(2+\tfrac{2}{3}x)\ \mathrm{NADPH}+(2-\tfrac{1}{3}x)\mathrm{FADH}_2. \end{aligned} \qquad [S49]$$

Note that by setting $x = 0$ in Eqs. [S*48*] and [S*49*], we get back the stoichiometry for fermentation and respiration as illustrated in Extended Data Figure 2, respectively.

Next, following the procedures described in Supplementary Notes 1-2, for a given value of x, we obtain the fluxes for the two energy pathways and also the biomass synthesis pathway (for the bioreactor series), and estimated proteome fractions for the two energy pathways by partitioning the protein abundances by the fluxes through the three pathways. In Table N4 the case of $x = 0$ is presented and Table N5 summarizes the results for $x = 20\%$.

Table N5: Partition of protein mass among the pathways for $x = 20\%$. Table is available as an appendix at the end of this SI. Column B lists the gene names for the 84 proteins, with 10 in the pentose phosphate pathway. Column A lists the pathway or the protein complex for the corresponding proteins. Columns C-E list the stoichiometry for the three pathways. The stoichiometry for the biomass synthesis pathway is based on Table 5 in Chapter 5 of the reference and on the assumption that x fraction of the total flux going to biomass synthesis takes the pentose phosphate pathway. The stoichiometry for each of the energy pathways is given by either Eq. [S48] or [S49]. Columns F-L list for the condition of NQ381 with 400 μM 3MBA the protein abundances (Column F), fluxes (Columns G-I), and protein mass allocated to each of the three pathways (Columns J-L). The format of the data is similar for the other 3 growth conditions, i.e., NQ381 with 500 (Columns M-S) and 800 μM 3MBA (Columns T-Z), and WT NCM3722 in lactose minimal medium (Columns AA-AG).

With flux and proteome fraction data, values of the model parameters for various values of x can be obtained following procedures in Sec. D of Supplementary Note 1. The results are shown in Table N6. It is clear from the results that the model parameters do not have strong dependence on x, validating results based on the simplified model of central metabolism.

Parameter (Units)	$x = 0$	$x = 20\%$	$x = 50\%$	$x = 80\%$
$\phi_{E,\max}=1-\phi_0$ (%)	18.7±1.2	18.9±1.3	19.2±1.3	19.6±1.3
b (% hr)	11.5±1.3	11.6±1.4	12.0±1.5	12.5±1.5
σ (mM/OD)	45.6±2.9	45.5±2.9	45.2±2.9	44.9±2.9
e_f (1)	2.0	2.1	2.2	2.3
e_r (1)	4.4	4.4	4.4	4.3
ε_f (mM/OD/hr)	748±30	735±28	760±28	781±27
ε_r (mM/OD/hr)	393±12	383±15	373±21	362±27
β (mM/OD)	28.5±1.3	28.5±1.3	28.5±1.3	28.5±1.3

Table N6: Effect of the inclusion of the pentose phosphate pathway on model parameters. See Extended Data Table 2 and Supplementary Note 1 for the description of model parameters. The values of the parameters are listed for four different values of x. All parameters have variations less than 10%, with most having even less variation.

An important prediction of the model is the increase of the respiration CO_2 flux while acetate excretion decreases under carbon limitation. With the inclusion of the pentose phosphate pathway, Eq. [S*43*] becomes

$$J_{CO2,r} = J_{CO2} - (1 + \frac{3x}{6-x})J_{ac} - \beta_{CO2} \cdot \lambda \,, \qquad \text{[S50]}$$

where we have used the new stoichiometry between acetate and CO_2 for the fermentation pathway given by Eq. [S*48*], i.e., $J_{CO2,f} = \frac{6+2x}{6-x} J_{ac}$. The resulting estimates for $J_{CO2,r}$ are shown in Figure N10 for $x = 20\%$. Also shown are the model descriptions based on the corresponding model parameters given in Table N6. Both the striking increase of respiration CO_2 flux and the good agreement between the data and model description prove that the value of x has little influence on our main results.

The small effect of the inclusion of the pentose phosphate pathway can be understood intuitively by comparing the proteome fractions of the pentose phosphate pathway, upper glycolysis, and lower glycolysis (Figure N15a) As shown in Figure N15b, lower glycolysis has a much larger proteome fraction, which makes whatever variations the upper part has (due to the alternative pathway) not significant.

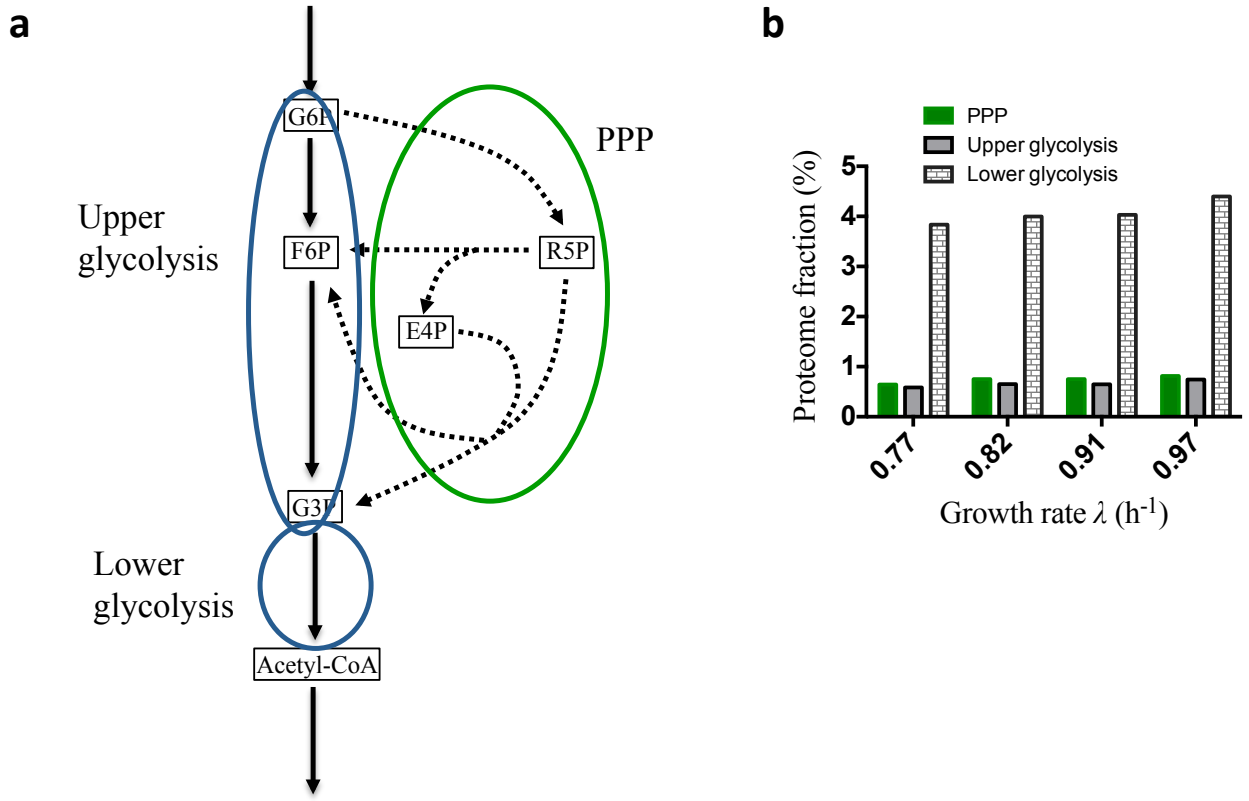

Figure N15: Proteome fractions of the pentose phosphate pathway, upper glycolysis, and lower glycolysis. a. The proteins for upper glycolysis include enzymes catalyzing the glycolysis pathway starting from G6P and ending with G3P, and the proteins for lower glycolysis include enzymes downstream from G3P to Acetyl-CoA. The proteins in the pentose phosphate pathway (PPP) include all enzymes involved in the pathway. An arrow can indicate multiple reactions (and thus multiple enzymes). **b.** The proteome fraction for each of the three groups of proteins in the four bioreactor conditions, with x-axis indicating the growth rate in the bioreactor series.

Supplementary References

1 Scott, M., Gunderson, C. W., Mateescu, E. M., Zhang, Z. & Hwa, T. Interdependence of cell growth and gene expression: origins and consequences. *Science* **330**, 1099-1102, doi:10.1126/science.1192588 (2010).

2 You, C. *et al.* Coordination of bacterial proteome with metabolism by cyclic AMP signalling. *Nature* **500**, 301-306, doi:10.1038/nature12446 (2013).

3 Hui, S. *et al.* Quantitative proteomic analysis reveals a simple strategy of global resource allocation in bacteria. *Mol Syst Biol* **11**, 784, doi:10.15252/msb.20145697 (2015).

4 Fischer, E. & Sauer, U. A novel metabolic cycle catalyzes glucose oxidation and anaplerosis in hungry Escherichia coli. *J Biol Chem* **278**, 46446-46451, doi:10.1074/jbc.M307968200 (2003).

5 Berkhout, J., Bruggeman, F. J. & Teusink, B. Optimality principles in the regulation of metabolic networks. *Metabolites* **2**, 529-552, doi:10.3390/metabo2030529 (2012).

6 Varma, A. & Palsson, B. O. Metabolic Flux Balancing: Basic Concepts, Scientic and Practical Use. *Bio/Technology* **12** (1994).

7 Neidhardt, F. C., Ingraham, J. L. & Schaechter, M. *Physiology of the Bacterial Cell: A Molecular Approach*. (Sinauer Associates Inc, 1990).

8 Reitzer, L. Nitrogen assimilation and global regulation in Escherichia coli. *Annu Rev Microbiol* **57**, 155-176, doi:10.1146/annurev.micro.57.030502.090820 (2003).

9 Perasso, R., Curgy, J.-J., Stelly, N. & Andre, J. Effects of chloramphenicol on the mitochondrial respiratory chain in the wild strain and in a cytoplasmic chloramphenicol-resistant mutant of Tetrahymena pyriformis. *Molecular and cellular biology* **2**, 715-719 (1982).

10 McKee, E., Ferguson, M., Bentley, A. & Marks, T. Inhibition of mammalian mitochondrial protein synthesis by oxazolidinones. *Antimicrobial agents and chemotherapy* **50**, 2042-2049 (2006).

11 Unden, G. & Dunnwald, P. 3.2.2 The Aerobic and Anaerobic Respiratory Chain of Escherichia coli and Salmonella enterica: Enzymes and Energetics. *EcoSal*, 1-65 (2008).

12 Kayser, A., Weber, J., Hecht, V. & Rinas, U. Metabolic flux analysis of Escherichia coli in glucose-limited continuous culture. I. Growth-rate-dependent metabolic efficiency at steady state. *Microbiology* **151**, 693-706, doi:10.1099/mic.0.27481-0 (2005).

13 Feist, A. M. *et al.* A genome-scale metabolic reconstruction for Escherichia coli K-12 MG1655 that accounts for 1260 ORFs and thermodynamic information. *Mol Syst Biol* **3**, 121, doi:10.1038/msb4100155 (2007).

14 Li, G. W., Burkhardt, D., Gross, C. & Weissman, J. S. Quantifying absolute protein synthesis rates reveals principles underlying allocation of cellular resources. *Cell* **157**, 624-635, doi:10.1016/j.cell.2014.02.033 (2014).

15 Bantscheff, M., Schirle, M., Sweetman, G., Rick, J. & Kuster, B. Quantitative mass spectrometry in proteomics: a critical review. *Anal Bioanal Chem* **389**, 1017-1031, doi:10.1007/s00216-007-1486-6 (2007).

16 Naftalin, R. J., Green, N. & Cunningham, P. Lactose permease H+-lactose symporter: mechanical switch or Brownian ratchet? *Biophys J* **92**, 3474-3491, doi:10.1529/biophysj.106.100669 (2007).
17 Seaver, L. C. & Imlay, J. A. Are respiratory enzymes the primary sources of intracellular hydrogen peroxide? *J Biol Chem* **279**, 48742-48750, doi:10.1074/jbc.M408754200 (2004).
18 Sauer, U., Canonaco, F., Heri, S., Perrenoud, A. & Fischer, E. The soluble and membrane-bound transhydrogenases UdhA and PntAB have divergent functions in NADPH metabolism of Escherichia coli. *J Biol Chem* **279**, 6613 (2004).
19 Nanchen, A., Schicker, A. & Sauer, U. Nonlinear dependency of intracellular fluxes on growth rate in miniaturized continuous cultures of Escherichia coli. *Appl Environ Microbiol* **72**, 1164-1172, doi:10.1128/AEM.72.2.1164-1172.2006 (2006).

Table N1

		Relative abundance					Ribosomal profiling	Absolute abundance				
		EQ353	NQ381 (400)	NQ381 (500)	NQ381 (800)	NCM3722	EQ353	NQ381 (400)	NQ381 (500)	NQ381 (800)	NCM3722	Note
Pathway or protein complex	**Gene**							13.46%	13.54%	12.49%	12.21%	Sum
Lactose degradation	lacY						0.000%					
	lacZ		1.05	1.09	1.10	0.96	0.001%	0.85%	0.88%	0.89%	0.78%	
	glk	0.67	0.87	1.08	0.92	0.87	0.013%	0.02%	0.02%	0.02%	0.02%	
	pgm						0.051%					
	galM	0.31	0.89	0.84	0.87	0.88	0.027%	0.08%	0.07%	0.08%	0.08%	
	galK		0.96	1.08	1.09	0.92	0.007%					
	galT						0.004%					
	galE		0.73	0.75	0.99	1.11	0.019%					
Glycolysis	pgi	1.63	0.95	0.97	1.08	1.16	0.149%	0.09%	0.09%	0.10%	0.11%	
	pfkA	1.13	1.00	1.02	1.02	1.03	0.069%	0.06%	0.06%	0.06%	0.06%	
	pfkB						0.029%					
	fbaA	1.31	1.08	1.19	1.20	1.34	0.382%	0.32%	0.35%	0.35%	0.39%	
	fbaB						0.073%					
	tpiA	1.08	0.88	1.13	0.98	1.34	0.148%	0.12%	0.15%	0.13%	0.18%	
	gapA	1.27	1.03	1.12	1.15	1.28	1.467%	1.19%	1.29%	1.33%	1.47%	
	pgk	1.16	0.99	1.02	1.05	1.19	0.351%	0.30%	0.31%	0.32%	0.36%	
	gpmA	1.52	1.07	1.05	1.06	1.12	0.220%	0.15%	0.15%	0.15%	0.16%	
	gpmI	1.44	1.04	1.08	1.26	1.42	0.111%	0.08%	0.08%	0.10%	0.11%	
	eno	1.10	1.03	1.14	1.21	1.35	0.678%	0.63%	0.70%	0.75%	0.83%	
	pykF	1.42	0.96	1.00	1.17	1.37	0.219%	0.15%	0.15%	0.18%	0.21%	
	pykA		1.17	1.09	0.97	0.97	0.058%					
	aceE	1.21	0.91	0.96	1.01	1.22	0.407%	0.30%	0.32%	0.34%	0.41%	
	aceF	1.12	0.97	1.11	1.13	1.15	0.241%	0.21%	0.24%	0.24%	0.25%	
	lpdA	0.68	1.16	1.12	1.02	0.96	0.374%	0.63%	0.61%	0.56%	0.52%	
	pta	0.73	1.08	1.11	1.09	1.06	0.066%	0.10%	0.10%	0.10%	0.10%	
	ackA						0.036%					
TCA	gltA	0.45	1.39	1.26	0.96	0.75	0.286%	0.88%	0.80%	0.61%	0.48%	
	acnA						0.059%					
	acnB	0.69	1.26	1.16	0.91	0.78	0.503%	0.92%	0.84%	0.66%	0.57%	
	icd	0.89	1.11	1.11	0.93	0.99	1.244%	1.55%	1.55%	1.31%	1.39%	
	sucA	0.50	1.07	1.17	0.94	0.82	0.156%	0.33%	0.36%	0.29%	0.25%	
	sucB	0.50	1.08	1.11	1.00	0.86	0.175%	0.38%	0.39%	0.35%	0.30%	
	lpdA	0.68	1.16	1.12	1.02	0.96	0.374%	0.63%	0.61%	0.56%	0.52%	
	sucC	0.43	1.23	1.16	0.89	0.71	0.185%	0.52%	0.49%	0.38%	0.30%	
	sucD	0.45	1.23	1.19	0.96	0.73	0.133%	0.36%	0.35%	0.28%	0.22%	
	sdhA	0.54	1.15	1.05	0.99	0.83	0.154%	0.33%	0.30%	0.29%	0.24%	
	sdhB	0.52	1.10	1.06	0.92	0.78	0.075%	0.16%	0.15%	0.13%	0.11%	
	sdhC						0.036%					
	sdhD						0.023%					
	fumA	0.45	1.28	1.11	0.90	0.70	0.083%	0.24%	0.21%	0.17%	0.13%	
	fumB						0.001%					
	fumC						0.015%					
	mdh	1.05	1.29	1.29	1.18	1.12	0.365%	0.45%	0.45%	0.41%	0.39%	
	ppc	1.83	0.93	1.07	1.07	1.14	0.308%	0.16%	0.18%	0.18%	0.19%	
NADH:ubiquinone oxidoreductase I (NDH-1)	nuoA						0.012%	0.02%	0.02%	0.02%	0.01%	Protein complex stoichiometry
	nuoB						0.028%	0.04%	0.04%	0.03%	0.03%	Protein complex stoichiometry
	nuoC	0.76	1.10	1.07	0.93	0.81	0.053%	0.08%	0.07%	0.06%	0.06%	
	nuoE						0.021%	0.03%	0.03%	0.03%	0.02%	Protein complex stoichiometry
	nuoF						0.036%	0.05%	0.05%	0.04%	0.04%	Protein complex stoichiometry
	nuoG						0.082%	0.12%	0.12%	0.10%	0.09%	Protein complex stoichiometry
	nuoH						0.016%	0.02%	0.02%	0.02%	0.02%	Protein complex stoichiometry
	nuoI						0.013%	0.02%	0.02%	0.02%	0.01%	Protein complex stoichiometry
	nuoJ						0.007%	0.01%	0.01%	0.01%	0.01%	Protein complex stoichiometry
	nuoK						0.005%	0.01%	0.01%	0.01%	0.00%	Protein complex stoichiometry
	nuoL						0.024%	0.03%	0.03%	0.03%	0.03%	Protein complex stoichiometry
	nuoM						0.023%	0.03%	0.03%	0.03%	0.02%	Protein complex stoichiometry
	nuoN						0.025%	0.04%	0.03%	0.03%	0.03%	Protein complex stoichiometry
NADH:ubiquinone oxidoreductase II (NDH-2)	ndh						0.029%					
cytochrome *bo* oxidase (CyoABCD)	cyoA						0.083%					
	cyoB						0.113%					
	cyoC						0.043%					
	cyoD						0.037%					
cytochrome *bd*-I oxidase (CydABX)	cydA						0.025%					
	cydB						0.013%					
	cydX						0.004%					
cytochrome *bd*-II oxidase (AppCB)	appC						0.001%					
	appB						0.000%					
F_1 complex of ATP synthase	atpA	0.81	1.12	1.11	1.04	0.99	0.369%	0.51%	0.51%	0.47%	0.45%	
	atpC						0.038%	0.05%	0.05%	0.05%	0.05%	Protein complex stoichiometry
	atpD	0.86	1.18	1.12	1.10	0.97	0.289%	0.40%	0.38%	0.37%	0.33%	
	atpG	0.83	1.21	1.11	0.96	0.85	0.069%	0.10%	0.09%	0.08%	0.07%	
	atpH	0.89	1.01	1.15	1.21	0.98	0.036%	0.04%	0.05%	0.05%	0.04%	
F_0 complex of ATP synthase	atpB						0.074%	0.08%	0.08%	0.08%	0.08%	Protein complex stoichiometry
	atpE						0.136%	0.15%	0.15%	0.15%	0.15%	Protein complex stoichiometry
	atpF	1.02	1.11	1.11	1.12	1.12	0.054%	0.06%	0.06%	0.06%	0.06%	

Table N2

		Spectral counting data for proteins with no assigned values in Table N1					Spectral counting data for proteins with estimated results in Table N1				
		EQ353	NQ381 (400)	NQ381 (500)	NQ381 (800)	NCM3722	EQ353	NQ381 (400)	NQ381 (500)	NQ381 (800)	NCM3722
Pathway or protein complex	**Gene**	**0.20%**	**0.65%**	**0.62%**	**0.74%**	**0.55%**	**13.53%**	**19.58%**	**18.20%**	**20.58%**	**17.24%**
Lactose degradation	lacY						0.00%	0.00%	0.00%	0.00%	0.00%
	lacZ						0.00%	0.89%	0.85%	0.83%	0.87%
	glk						0.03%	0.03%	0.07%	0.00%	0.10%
	pgm	0.03%	0.03%	0.00%	0.00%	0.00%					
	galM						0.00%	0.09%	0.10%	0.13%	0.10%
	galK	0.00%	0.18%	0.20%	0.22%	0.13%					
	galT	0.00%	0.03%	0.03%	0.03%	0.06%					
	galE	0.00%	0.15%	0.16%	0.29%	0.26%					
Glycolysis	pgi						0.24%	0.12%	0.16%	0.16%	0.22%
	pfkA						0.10%	0.06%	0.07%	0.00%	0.06%
	pfkB	0.03%	0.00%	0.00%	0.00%	0.00%					
	fbaA						0.60%	0.45%	0.36%	0.38%	0.51%
	fbaB	0.00%	0.00%	0.00%	0.00%	0.00%					
	tpiA						0.03%	0.06%	0.20%	0.03%	0.10%
	gapA						1.04%	0.83%	1.04%	0.96%	1.09%
	pgk						0.74%	0.74%	0.52%	0.61%	0.71%
	gpmA						0.47%	0.18%	0.26%	0.32%	0.32%
	gpmI						0.03%	0.03%	0.00%	0.03%	0.00%
	eno						0.64%	0.74%	0.81%	0.83%	0.96%
	pykF						0.20%	0.21%	0.07%	0.32%	0.42%
	pykA	0.10%	0.18%	0.13%	0.06%	0.06%					
	aceE						0.91%	0.71%	0.62%	0.80%	1.03%
	aceF						0.24%	0.27%	0.26%	0.26%	0.39%
	lpdA						0.64%	0.89%	0.88%	0.93%	0.90%
	pta						0.03%	0.21%	0.13%	0.06%	0.03%
	ackA	0.00%	0.06%	0.07%	0.06%	0.00%					
TCA	gltA						0.44%	0.92%	0.98%	0.58%	0.64%
	acnA	0.00%	0.03%	0.00%	0.00%	0.00%					
	acnB						0.40%	0.83%	0.91%	0.67%	0.45%
	icd						1.21%	1.64%	1.43%	1.22%	1.25%
	sucA						0.20%	0.48%	0.39%	0.45%	0.32%
	sucB						0.00%	0.18%	0.13%	0.29%	0.13%
	lpdA						0.64%	0.89%	0.88%	0.93%	0.90%
	sucC						0.60%	1.04%	1.20%	0.96%	0.90%
	sucD						0.13%	0.68%	0.62%	0.58%	0.35%
	sdhA						0.44%	0.95%	0.85%	0.96%	0.55%
	sdhB						0.30%	0.51%	0.52%	0.48%	0.42%
	sdhC	0.00%	0.00%	0.00%	0.00%	0.00%					
	sdhD	0.00%	0.00%	0.00%	0.00%	0.00%					
	fumA						0.07%	0.12%	0.16%	0.10%	0.10%
	fumB	0.00%	0.00%	0.00%	0.00%	0.00%					
	fumC	0.00%	0.00%	0.00%	0.00%	0.00%					
	mdh						1.14%	2.71%	1.50%	4.91%	1.44%
	ppc						0.50%	0.21%	0.23%	0.22%	0.22%
NADH:ubiquinone oxidoreductase I (NDH-1)	nuoA						0.00%	0.00%	0.00%	0.00%	0.00%
	nuoB						0.03%	0.00%	0.00%	0.00%	0.00%
	nuoC						0.10%	0.18%	0.10%	0.10%	0.10%
	nuoE						0.00%	0.00%	0.00%	0.00%	0.00%
	nuoF						0.00%	0.06%	0.07%	0.03%	0.00%
	nuoG						0.03%	0.06%	0.13%	0.03%	0.00%
	nuoH						0.00%	0.00%	0.00%	0.00%	0.00%
	nuoI						0.00%	0.00%	0.03%	0.00%	0.00%
	nuoJ						0.00%	0.00%	0.00%	0.00%	0.00%
	nuoK						0.00%	0.00%	0.00%	0.00%	0.00%
	nuoL						0.00%	0.00%	0.00%	0.00%	0.00%
	nuoM						0.00%	0.00%	0.00%	0.00%	0.00%
	nuoN						0.00%	0.00%	0.00%	0.00%	0.00%
NADH:ubiquinone oxidoreductase II (NDH-2)	ndh	0.00%	0.00%	0.00%	0.03%	0.00%					
cytochrome *bo* oxidase (CyoABCD)	cyoA	0.03%	0.00%	0.03%	0.03%	0.03%					
	cyoB	0.00%	0.00%	0.00%	0.00%	0.00%					
	cyoC	0.00%	0.00%	0.00%	0.00%	0.00%					
	cyoD	0.00%	0.00%	0.00%	0.00%	0.00%					
cytochrome *bd*-I oxidase (CydABX)	cydA	0.00%	0.00%	0.00%	0.00%	0.00%					
	cydB	0.00%	0.00%	0.00%	0.00%	0.00%					
	cydX	0.00%	0.00%	0.00%	0.00%	0.00%					
cytochrome *bd*-II oxidase (AppCB)	appC	0.00%	0.00%	0.00%	0.00%	0.00%					
	appB	0.00%	0.00%	0.00%	0.00%	0.00%					
F_1 complex of ATP synthase	atpA						0.87%	1.22%	1.04%	1.06%	1.12%
	atpC						0.00%	0.00%	0.00%	0.00%	0.00%
	atpD						0.81%	0.98%	1.07%	0.87%	0.93%
	atpG						0.13%	0.15%	0.10%	0.13%	0.19%
	atpH						0.10%	0.00%	0.10%	0.13%	0.10%
F_0 complex of ATP synthase	atpB						0.00%	0.00%	0.00%	0.00%	0.00%
	atpE						0.00%	0.03%	0.00%	0.03%	0.00%
	atpF						0.07%	0.12%	0.26%	0.13%	0.22%

Table N3

		Absolute abundance				
		NQ381 (400)	NQ381 (500)	NQ381 (800)	NCM3722	Method of estimate
Pathway or protein complex	**Gene**	**14.33%**	**14.38%**	**13.54%**	**13.08%**	**Sum**
Lactose degradation	lacY	0.22%	0.22%	0.31%	0.33%	Enzyme kinetics; assuming a turnover rate of 20 s-1 for the lactose permease.
	lacZ	0.85%	0.88%	0.89%	0.78%	
	glk	0.02%	0.02%	0.02%	0.02%	
	pgm	0.03%	0.00%	0.00%	0.00%	Spectral counting
	galM	0.08%	0.07%	0.08%	0.08%	
	galK	0.18%	0.20%	0.22%	0.13%	Spectral counting
	galT	0.03%	0.03%	0.03%	0.06%	Spectral counting
	galE	0.15%	0.16%	0.29%	0.26%	Spectral counting
Glycolysis	pgi	0.09%	0.09%	0.10%	0.11%	
	pfkA	0.06%	0.06%	0.06%	0.06%	
	pfkB	0.00%	0.00%	0.00%	0.00%	Spectral counting
	fbaA	0.32%	0.35%	0.35%	0.39%	
	fbaB	0.00%	0.00%	0.00%	0.00%	Spectral counting
	tpiA	0.12%	0.15%	0.13%	0.18%	
	gapA	1.19%	1.29%	1.33%	1.47%	
	pgk	0.30%	0.31%	0.32%	0.36%	
	gpmA	0.15%	0.15%	0.15%	0.16%	
	gpmI	0.08%	0.08%	0.10%	0.11%	
	eno	0.63%	0.70%	0.75%	0.83%	
	pykF	0.15%	0.15%	0.18%	0.21%	
	pykA	0.18%	0.13%	0.06%	0.06%	Spectral counting
	aceE	0.30%	0.32%	0.34%	0.41%	
	aceF	0.21%	0.24%	0.24%	0.25%	
	lpdA	0.63%	0.61%	0.56%	0.52%	
	pta	0.10%	0.10%	0.10%	0.10%	
	ackA	0.06%	0.07%	0.06%	0.00%	Spectral counting
TCA	gltA	0.88%	0.80%	0.61%	0.48%	
	acnA	0.03%	0.00%	0.00%	0.00%	Spectral counting
	acnB	0.92%	0.84%	0.66%	0.57%	
	icd	1.55%	1.55%	1.31%	1.39%	
	sucA	0.33%	0.36%	0.29%	0.25%	
	sucB	0.38%	0.39%	0.35%	0.30%	
	lpdA	0.63%	0.61%	0.56%	0.52%	
	sucC	0.52%	0.49%	0.38%	0.30%	
	sucD	0.36%	0.35%	0.28%	0.22%	
	sdhA	0.33%	0.30%	0.29%	0.24%	
	sdhB	0.16%	0.15%	0.13%	0.11%	
	sdhC	0.00%	0.00%	0.00%	0.00%	Spectral counting
	sdhD	0.00%	0.00%	0.00%	0.00%	Spectral counting
	fumA	0.24%	0.21%	0.17%	0.13%	
	fumB	0.00%	0.00%	0.00%	0.00%	Spectral counting
	fumC	0.00%	0.00%	0.00%	0.00%	Spectral counting
	mdh	0.45%	0.45%	0.41%	0.39%	
	ppc	0.16%	0.18%	0.18%	0.19%	
NADH:ubiquinone oxidoreductase I (NDH-1)	nuoA	0.02%	0.02%	0.02%	0.01%	
	nuoB	0.04%	0.04%	0.03%	0.03%	
	nuoC	0.08%	0.07%	0.06%	0.06%	
	nuoE	0.03%	0.03%	0.03%	0.02%	
	nuoF	0.05%	0.05%	0.04%	0.04%	
	nuoG	0.12%	0.12%	0.10%	0.09%	
	nuoH	0.02%	0.02%	0.02%	0.02%	
	nuoI	0.02%	0.02%	0.02%	0.01%	
	nuoJ	0.01%	0.01%	0.01%	0.01%	
	nuoK	0.01%	0.01%	0.01%	0.00%	
	nuoL	0.03%	0.03%	0.03%	0.03%	
	nuoM	0.03%	0.03%	0.03%	0.02%	
	nuoN	0.04%	0.03%	0.03%	0.03%	
NADH:ubiquinone oxidoreductase II (NDH-2)	ndh	0.00%	0.00%	0.03%	0.00%	Spectral counting
cytochrome *bo* oxidase (CyoABCD)	cyoA	0.00%	0.03%	0.03%	0.03%	Spectral counting
	cyoB	0.00%	0.00%	0.00%	0.00%	Spectral counting
	cyoC	0.00%	0.00%	0.00%	0.00%	Spectral counting
	cyoD	0.00%	0.00%	0.00%	0.00%	Spectral counting
cytochrome *bd*-I oxidase (CydABX)	cydA	0.00%	0.00%	0.00%	0.00%	Spectral counting
	cydB	0.00%	0.00%	0.00%	0.00%	Spectral counting
	cydX	0.00%	0.00%	0.00%	0.00%	Spectral counting
cytochrome *bd*-II oxidase (AppCB)	appC	0.00%	0.00%	0.00%	0.00%	Spectral counting
	appB	0.00%	0.00%	0.00%	0.00%	Spectral counting
F_1 complex of ATP synthase	atpA	0.51%	0.51%	0.47%	0.45%	
	atpC	0.05%	0.05%	0.05%	0.05%	
	atpD	0.40%	0.38%	0.37%	0.33%	
	atpG	0.10%	0.09%	0.08%	0.07%	
	atpH	0.04%	0.05%	0.05%	0.04%	
F_0 complex of ATP synthase	atpB	0.08%	0.08%	0.08%	0.08%	
	atpE	0.15%	0.15%	0.15%	0.15%	
	atpF	0.06%	0.06%	0.06%	0.06%	

Table N4

					NQ381 (400)							NQ381 (500)							NQ381 (800)							NCM3722						
		Pathway stoichiometry				Flux through pathway			Protein mass allocated to pathway				Flux through pathway			Protein mass allocated to pathway				Flux through pathway			Protein mass allocated to pathway				Flux through pathway			Protein mass allocated to pathway		
Pathway or protein complex	Gene	Biomass ($S_{p,BM}$)	Fermentation ($S_{p,f}$)	Respiration ($S_{p,r}$)	Protein abundance (ϕ_p)	Biomass ($J_{p,BM}$)	Fermentation ($J_{p,f}$)	Respiration ($J_{p,r}$)	Biomass ($\phi_{p,BM}$)	Fermentation ($\phi_{p,f}$)	Respiration ($\phi_{p,r}$)	Protein abundance (ϕ_p)	Biomass ($J_{p,BM}$)	Fermentation ($J_{p,f}$)	Respiration ($J_{p,r}$)	Biomass ($\phi_{p,BM}$)	Fermentation ($\phi_{p,f}$)	Respiration ($\phi_{p,r}$)	Protein abundance (ϕ_p)	Biomass ($J_{p,BM}$)	Fermentation ($J_{p,f}$)	Respiration ($J_{p,r}$)	Biomass ($\phi_{p,BM}$)	Fermentation ($\phi_{p,f}$)	Respiration ($\phi_{p,r}$)	Protein abundance (ϕ_p)	Biomass ($J_{p,BM}$)	Fermentation ($J_{p,f}$)	Respiration ($J_{p,r}$)	Biomass ($\phi_{p,BM}$)	Fermentation ($\phi_{p,f}$)	Respiration ($\phi_{p,r}$)
					14.33%				4.12%	0.58%	9.64%	14.38%				4.95%	1.30%	8.12%	13.54%				4.75%	2.62%	6.17%	13.08%				5.44%	2.72%	4.91%
Lactose degradation	lacY	1	1	1	0.22%	1.56	0.11	0.71	0.14%	0.01%	0.07%	0.22%	2.15	0.34	0.57	0.16%	0.02%	0.04%	0.31%	2.10	0.77	0.41	0.20%	0.07%	0.04%	0.33%	2.36	0.81	0.29	0.22%	0.08%	0.03%
	lacZ	1	1	1	0.85%	1.56	0.11	0.71	0.56%	0.04%	0.25%	0.88%	2.15	0.34	0.57	0.62%	0.10%	0.16%	0.89%	2.10	0.77	0.41	0.57%	0.21%	0.11%	0.78%	2.36	0.81	0.29	0.53%	0.18%	0.07%
	glk	1	1	1	0.02%	1.56	0.11	0.71	0.01%	0.00%	0.01%	0.02%	2.15	0.34	0.57	0.01%	0.00%	0.00%	0.02%	2.10	0.77	0.41	0.01%	0.00%	0.00%	0.02%	2.36	0.81	0.29	0.01%	0.00%	0.00%
	pgm	1	1	1	0.03%	1.56	0.11	0.71	0.02%	0.00%	0.01%	0.00%	2.15	0.34	0.57	0.00%	0.00%	0.00%	0.00%	2.10	0.77	0.41	0.00%	0.00%	0.00%	0.00%	2.36	0.81	0.29	0.00%	0.00%	0.00%
	galM	1	1	1	0.08%	1.56	0.11	0.71	0.05%	0.00%	0.02%	0.07%	2.15	0.34	0.57	0.05%	0.01%	0.01%	0.08%	2.10	0.77	0.41	0.05%	0.02%	0.01%	0.08%	2.36	0.81	0.29	0.05%	0.02%	0.01%
	galK	1	1	1	0.18%	1.56	0.11	0.71	0.12%	0.01%	0.05%	0.20%	2.15	0.34	0.57	0.14%	0.02%	0.04%	0.22%	2.10	0.77	0.41	0.14%	0.05%	0.03%	0.13%	2.36	0.81	0.29	0.09%	0.03%	0.01%
	galT	1	1	1	0.03%	1.56	0.11	0.71	0.02%	0.00%	0.01%	0.03%	2.15	0.34	0.57	0.02%	0.00%	0.01%	0.03%	2.10	0.77	0.41	0.02%	0.01%	0.00%	0.06%	2.36	0.81	0.29	0.04%	0.02%	0.01%
	galE	1	1	1	0.15%	1.56	0.11	0.71	0.10%	0.01%	0.04%	0.16%	2.15	0.34	0.57	0.11%	0.02%	0.03%	0.29%	2.10	0.77	0.41	0.18%	0.07%	0.04%	0.26%	2.36	0.81	0.29	0.18%	0.06%	0.02%
Glycolysis	pgi	1.628	2	2	0.09%	2.54	0.22	1.42	0.05%	0.00%	0.03%	0.09%	3.50	0.68	1.14	0.06%	0.01%	0.02%	0.10%	3.42	1.54	0.82	0.06%	0.03%	0.01%	0.11%	3.84	1.62	0.58	0.07%	0.03%	0.01%
	pfkA	1.61	2	2	0.06%	2.51	0.22	1.42	0.04%	0.00%	0.02%	0.06%	3.46	0.68	1.14	0.04%	0.01%	0.01%	0.06%	3.38	1.54	0.82	0.04%	0.02%	0.01%	0.06%	3.80	1.62	0.58	0.04%	0.02%	0.01%
	pfkB	1.61	2	2	0.00%	2.51	0.22	1.42	0.00%	0.00%	0.00%	0.00%	3.46	0.68	1.14	0.00%	0.00%	0.00%	0.00%	3.38	1.54	0.82	0.00%	0.00%	0.00%	0.00%	3.80	1.62	0.58	0.00%	0.00%	0.00%
	fbaA	1.61	2	2	0.32%	2.51	0.22	1.42	0.19%	0.02%	0.11%	0.35%	3.46	0.68	1.14	0.23%	0.04%	0.08%	0.35%	3.38	1.54	0.82	0.21%	0.09%	0.05%	0.39%	3.80	1.62	0.58	0.25%	0.11%	0.04%
	fbaB	1.61	2	2	0.00%	2.51	0.22	1.42	0.00%	0.00%	0.00%	0.00%	3.46	0.68	1.14	0.00%	0.00%	0.00%	0.00%	3.38	1.54	0.82	0.00%	0.00%	0.00%	0.00%	3.80	1.62	0.58	0.00%	0.00%	0.00%
	tpiA	1.61	2	2	0.12%	2.51	0.22	1.42	0.07%	0.01%	0.04%	0.15%	3.46	0.68	1.14	0.10%	0.02%	0.03%	0.13%	3.38	1.54	0.82	0.08%	0.04%	0.02%	0.18%	3.80	1.62	0.58	0.12%	0.05%	0.02%
	gapA	3.188	4	4	1.19%	4.97	0.44	2.84	0.72%	0.06%	0.41%	1.29%	6.85	1.36	2.28	0.84%	0.17%	0.28%	1.33%	6.69	3.08	1.64	0.78%	0.36%	0.19%	1.47%	7.52	3.24	1.16	0.93%	0.40%	0.14%
	pgk	3.188	4	4	0.30%	4.97	0.44	2.84	0.18%	0.02%	0.10%	0.31%	6.85	1.36	2.28	0.20%	0.04%	0.07%	0.32%	6.69	3.08	1.64	0.19%	0.09%	0.05%	0.36%	7.52	3.24	1.16	0.23%	0.10%	0.04%
	gpmA	2.808	4	4	0.15%	4.38	0.44	2.84	0.09%	0.01%	0.06%	0.15%	6.04	1.36	2.28	0.10%	0.02%	0.04%	0.15%	5.90	3.08	1.64	0.08%	0.04%	0.02%	0.16%	6.63	3.24	1.16	0.10%	0.05%	0.02%
	gpmI	2.808	4	4	0.08%	4.38	0.44	2.84	0.05%	0.00%	0.03%	0.08%	6.04	1.36	2.28	0.05%	0.01%	0.02%	0.10%	5.90	3.08	1.64	0.05%	0.03%	0.01%	0.11%	6.63	3.24	1.16	0.07%	0.03%	0.01%
	eno	2.808	4	4	0.63%	4.38	0.44	2.84	0.36%	0.04%	0.23%	0.70%	6.04	1.36	2.28	0.44%	0.10%	0.17%	0.75%	5.90	3.08	1.64	0.41%	0.22%	0.12%	0.83%	6.63	3.24	1.16	0.50%	0.24%	0.09%
	pykF	1.948	4	4	0.15%	3.04	0.44	2.84	0.07%	0.01%	0.07%	0.15%	4.19	1.36	2.28	0.08%	0.03%	0.05%	0.18%	4.09	3.08	1.64	0.08%	0.06%	0.03%	0.21%	4.60	3.24	1.16	0.11%	0.08%	0.03%
	pykA	1.948	4	4	0.18%	3.04	0.44	2.84	0.09%	0.01%	0.08%	0.13%	4.19	1.36	2.28	0.07%	0.02%	0.04%	0.06%	4.09	3.08	1.64	0.03%	0.02%	0.01%	0.06%	4.60	3.24	1.16	0.03%	0.02%	0.01%
	aceE	1.228	4	4	0.30%	1.92	0.44	2.84	0.11%	0.03%	0.17%	0.32%	2.64	1.36	2.28	0.14%	0.07%	0.12%	0.34%	2.58	3.08	1.64	0.12%	0.14%	0.08%	0.41%	2.90	3.24	1.16	0.16%	0.18%	0.07%
	aceF	1.228	4	4	0.21%	1.92	0.44	2.84	0.08%	0.02%	0.11%	0.24%	2.64	1.36	2.28	0.10%	0.05%	0.09%	0.24%	2.58	3.08	1.64	0.09%	0.10%	0.05%	0.25%	2.90	3.24	1.16	0.10%	0.11%	0.04%
	lpdA	1.228	4	4	0.63%	1.92	0.44	2.84	0.15%	0.03%	0.22%	0.61%	2.64	1.36	2.28	0.19%	0.10%	0.16%	0.56%	2.58	3.08	1.64	0.16%	0.19%	0.10%	0.52%	2.90	3.24	1.16	0.18%	0.20%	0.07%
	pta	0	4	0	0.10%	0.00	0.44	0	0.00%	0.10%	0.00%	0.10%	0.00	1.36	0	0.00%	0.10%	0.00%	0.10%	0.00	3.08	0	0.00%	0.10%	0.00%	0.10%	0.00	3.24	0	0.00%	0.10%	0.00%
	ackA	0	4	0	0.06%	0.00	0.44	0	0.00%	0.06%	0.00%	0.07%	0.00	1.36	0	0.00%	0.07%	0.00%	0.06%	0.00	3.08	0	0.00%	0.06%	0.00%	0.00%	0.00	3.24	0	0.00%	0.00%	0.00%
TCA	gltA	0.274	0	4	0.88%	0.43	0	2.84	0.12%	0.00%	0.77%	0.80%	0.59	0	2.28	0.17%	0.00%	0.64%	0.61%	0.58	0	1.64	0.16%	0.00%	0.46%	0.48%	0.65	0	1.16	0.17%	0.00%	0.31%
	acnA	0.274	0	4	0.03%	0.43	0	2.84	0.00%	0.00%	0.03%	0.00%	0.59	0	2.28	0.00%	0.00%	0.00%	0.00%	0.58	0	1.64	0.00%	0.00%	0.00%	0.00%	0.65	0	1.16	0.00%	0.00%	0.00%
	acnB	0.274	0	4	0.92%	0.43	0	2.84	0.12%	0.00%	0.80%	0.84%	0.59	0	2.28	0.17%	0.00%	0.67%	0.66%	0.58	0	1.64	0.17%	0.00%	0.49%	0.57%	0.65	0	1.16	0.20%	0.00%	0.36%
	icd	0.274	0	4	1.55%	0.43	0	2.84	0.20%	0.00%	1.35%	1.55%	0.59	0	2.28	0.32%	0.00%	1.24%	1.31%	0.58	0	1.64	0.34%	0.00%	0.97%	1.39%	0.65	0	1.16	0.50%	0.00%	0.89%
	sucA	0	0	4	0.33%	0.00	0	2.84	0.00%	0.00%	0.33%	0.36%	0.00	0	2.28	0.00%	0.00%	0.36%	0.29%	0.00	0	1.64	0.00%	0.00%	0.29%	0.25%	0.00	0	1.16	0.00%	0.00%	0.25%
	sucB	0	0	4	0.38%	0.00	0	2.84	0.00%	0.00%	0.38%	0.39%	0.00	0	2.28	0.00%	0.00%	0.39%	0.35%	0.00	0	1.64	0.00%	0.00%	0.35%	0.30%	0.00	0	1.16	0.00%	0.00%	0.30%
	lpdA	0	0	4	0.63%	0.00	0	2.84	0.00%	0.00%	0.22%	0.61%	0.00	0	2.28	0.00%	0.00%	0.16%	0.56%	0.00	0	1.64	0.00%	0.00%	0.10%	0.52%	0.00	0	1.16	0.00%	0.00%	0.07%
	sucC	0	0	4	0.52%	0.00	0	2.84	0.00%	0.00%	0.52%	0.49%	0.00	0	2.28	0.00%	0.00%	0.49%	0.38%	0.00	0	1.64	0.00%	0.00%	0.38%	0.30%	0.00	0	1.16	0.00%	0.00%	0.30%
	sucD	0	0	4	0.36%	0.00	0	2.84	0.00%	0.00%	0.36%	0.35%	0.00	0	2.28	0.00%	0.00%	0.35%	0.28%	0.00	0	1.64	0.00%	0.00%	0.28%	0.22%	0.00	0	1.16	0.00%	0.00%	0.22%
	sdhA	0	0	4	0.33%	0.00	0	2.84	0.00%	0.00%	0.33%	0.30%	0.00	0	2.28	0.00%	0.00%	0.30%	0.29%	0.00	0	1.64	0.00%	0.00%	0.29%	0.24%	0.00	0	1.16	0.00%	0.00%	0.24%
	sdhB	0	0	4	0.16%	0.00	0	2.84	0.00%	0.00%	0.16%	0.15%	0.00	0	2.28	0.00%	0.00%	0.15%	0.13%	0.00	0	1.64	0.00%	0.00%	0.13%	0.11%	0.00	0	1.16	0.00%	0.00%	0.11%
	sdhC	0	0	4	0.00%	0.00	0	2.84	0.00%	0.00%	0.00%	0.00%	0.00	0	2.28	0.00%	0.00%	0.00%	0.00%	0.00	0	1.64	0.00%	0.00%	0.00%	0.00%	0.00	0	1.16	0.00%	0.00%	0.00%
	sdhD	0	0	4	0.00%	0.00	0	2.84	0.00%	0.00%	0.00%	0.00%	0.00	0	2.28	0.00%	0.00%	0.00%	0.00%	0.00	0	1.64	0.00%	0.00%	0.00%	0.00%	0.00	0	1.16	0.00%	0.00%	0.00%
	fumA	0	0	4	0.24%	0.00	0	2.84	0.00%	0.00%	0.24%	0.21%	0.00	0	2.28	0.00%	0.00%	0.21%	0.17%	0.00	0	1.64	0.00%	0.00%	0.17%	0.13%	0.00	0	1.16	0.00%	0.00%	0.13%
	fumB	0	0	4	0.00%	0.00	0	2.84	0.00%	0.00%	0.00%	0.00%	0.00	0	2.28	0.00%	0.00%	0.00%	0.00%	0.00	0	1.64	0.00%	0.00%	0.00%	0.00%	0.00	0	1.16	0.00%	0.00%	0.00%
	fumC	0	0	4	0.00%	0.00	0	2.84	0.00%	0.00%	0.00%	0.00%	0.00	0	2.28	0.00%	0.00%	0.00%	0.00%	0.00	0	1.64	0.00%	0.00%	0.00%	0.00%	0.00	0	1.16	0.00%	0.00%	0.00%
	mdh	0	0	4	0.45%	0.00	0	2.84	0.00%	0.00%	0.45%	0.45%	0.00	0	2.28	0.00%	0.00%	0.45%	0.41%	0.00	0	1.64	0.00%	0.00%	0.41%	0.39%	0.00	0	1.16	0.00%	0.00%	0.39%
	ppc	0.728	0	0	0.16%	1.14	0	0	0.16%	0.00%	0.00%	0.18%	1.57	0	0	0.18%	0.00%	0.00%	0.18%	1.53	0	0	0.18%	0.00%	0.00%	0.19%	1.72	0	0	0.19%	0.00%	0.00%
NADH:ubiquinone oxidoreductase I (NDH-1)	nuoA	1.678	8	22	0.02%	2.62	0.88	15.62	0.00%	0.00%	0.01%	0.02%	3.61	2.72	12.54	0.00%	0.00%	0.01%	0.02%	3.52	6.16	9.02	0.00%	0.01%	0.01%	0.01%	3.96	6.48	6.38	0.00%	0.01%	0.01%
	nuoB	1.678	8	22	0.04%	2.62	0.88	15.62	0.01%	0.00%	0.03%	0.04%	3.61	2.72	12.54	0.01%	0.01%	0.03%	0.03%	3.52	6.16	9.02	0.01%	0.01%	0.02%	0.03%	3.96	6.48	6.38	0.01%	0.01%	0.01%
	nuoC	1.678	8	22	0.08%	2.62	0.88	15.62	0.01%	0.00%	0.06%	0.07%	3.61	2.72	12.54	0.01%	0.01%	0.05%	0.06%	3.52	6.16	9.02	0.01%	0.02%	0.03%	0.06%	3.96	6.48	6.38	0.01%	0.02%	0.02%
	nuoE	1.678	8	22	0.03%	2.62	0.88	15.62	0.00%	0.00%	0.03%	0.03%	3.61	2.72	12.54	0.01%	0.00%	0.02%	0.03%	3.52	6.16	9.02	0.00%	0.01%	0.01%	0.02%	3.96	6.48	6.38	0.01%	0.01%	0.01%
	nuoF	1.678	8	22	0.05%	2.62	0.88	15.62	0.01%	0.00%	0.04%	0.05%	3.61	2.72	12.54	0.01%	0.01%	0.03%	0.04%	3.52	6.16	9.02	0.01%	0.01%	0.02%	0.04%	3.96	6.48	6.38	0.01%	0.01%	0.01%
	nuoG	1.678	8	22	0.12%	2.62	0.88	15.62	0.02%	0.01%	0.10%	0.12%	3.61	2.72	12.54	0.02%	0.02%	0.08%	0.10%	3.52	6.16	9.02	0.02%	0.03%	0.05%	0.09%	3.96	6.48	6.38	0.02%	0.03%	0.03%
	nuoH	1.678	8	22	0.02%	2.62	0.88	15.62	0.00%	0.00%	0.02%	0.02%	3.61	2.72	12.54	0.00%	0.00%	0.01%	0.02%	3.52	6.16	9.02	0.00%	0.01%	0.01%	0.02%	3.96	6.48	6.38	0.00%	0.01%	0.01%
	nuoI	1.678	8	22	0.02%	2.62	0.88	15.62	0.00%	0.00%	0.02%	0.02%	3.61	2.72	12.54	0.00%	0.00%	0.01%	0.02%	3.52	6.16	9.02	0.00%	0.01%	0.01%	0.01%	3.96	6.48	6.38	0.00%	0.01%	0.01%
	nuoJ	1.678	8	22	0.01%	2.62	0.88	15.62	0.00%	0.00%	0.01%	0.01%	3.61	2.72	12.54	0.00%	0.00%	0.01%	0.01%	3.52	6.16	9.02	0.00%	0.00%	0.00%	0.01%	3.96	6.48	6.38	0.00%	0.00%	0.00%
	nuoK	1.678	8	22	0.01%	2.62	0.88	15.62	0.00%	0.00%	0.01%	0.01%	3.61	2.72	12.54	0.00%	0.00%	0.00%	0.01%	3.52	6.16	9.02	0.00%	0.00%	0.00%	0.00%	3.96	6.48	6.38	0.00%	0.00%	0.00%
	nuoL	1.678	8	22	0.03%	2.62	0.88	15.62	0.00%	0.00%	0.03%	0.03%	3.61	2.72	12.54	0.01%	0.00%	0.02%	0.03%	3.52	6.16	9.02	0.01%	0.01%	0.01%	0.03%	3.96	6.48	6.38	0.01%	0.01%	0.01%
	nuoM	1.678	8	22	0.03%	2.62	0.88	15.62	0.00%	0.00%	0.03%	0.03%	3.61	2.72	12.54	0.01%	0.00%	0.02%	0.03%	3.52	6.16	9.02	0.01%	0.01%	0.01%	0.02%	3.96	6.48	6.38	0.01%	0.01%	0.01%
	nuoN	1.678	8	22	0.04%	2.62	0.88	15.62	0.00%	0.00%	0.03%	0.03%	3.61	2.72	12.54	0.01%	0.01%	0.02%	0.03%	3.52	6.16	9.02	0.01%	0.01%	0.01%	0.03%	3.96	6.48	6.38	0.01%	0.01%	0.01%
NADH:ubiquinone oxidoreductase II (NDH-2)	ndh	1.678	8	22	0.00%	2.62	0.88	15.62	0.00%	0.00%	0.00%	0.00%	3.61	2.72	12.54	0.00%	0.00%	0.00%	0.03%	3.52	6.16	9.02	0.01%	0.01%	0.02%	0.00%	3.96	6.48	6.38	0.00%	0.00%	0.00%
cytochrome *bo* oxidase (CyoABCD)	cyoA	1.678	8	22	0.00%	2.62	0.88	15.62	0.00%	0.00%	0.00%	0.03%	3.61	2.72	12.54	0.01%	0.00%	0.02%	0.03%	3.52	6.16	9.02	0.01%	0.01%	0.02%	0.03%	3.96	6.48	6.38	0.01%	0.01%	0.01%
	cyoB	1.678	8	22	0.00%	2.62	0.88	15.62	0.00%	0.00%	0.00%	0.00%	3.61	2.72	12.54	0.00%	0.00%	0.00%	0.00%	3.52	6.16	9.02	0.00%	0.00%	0.00%	0.00%	3.96	6.48	6.38	0.00%	0.00%	0.00%
	cyoC	1.678	8	22	0.00%	2.62	0.88	15.62	0.00%	0.00%	0.00%	0.00%	3.61	2.72	12.54	0.00%	0.00%	0.00%	0.00%	3.52	6.16	9.02	0.00%	0.00%	0.00%	0.00%	3.96	6.48	6.38	0.00%	0.00%	0.00%
	cyoD	1.678	8	22	0.00%	2.62	0.88	15.62	0.00%	0.00%	0.00%	0.00%	3.61	2.72	12.54	0.00%	0.00%	0.00%	0.00%	3.52	6.16	9.02	0.00%	0.00%	0.00%	0.00%	3.96	6.48	6.38	0.00%	0.00%	0.00%
cytochrome *bd*-I oxidase (CydABX)	cydA	1.678	8	22	0.00%	2.62	0.88	15.62	0.00%	0.00%	0.00%	0.00%	3.61	2.72	12.54	0.00%	0.00%	0.00%	0.00%	3.52	6.16	9.02	0.00%	0.00%	0.00%	0.00%	3.96	6.48	6.38	0.00%	0.00%	0.00%
	cydB	1.678	8	22	0.00%	2.62	0.88	15.62	0.00%	0.00%	0.00%	0.00%	3.61	2.72	12.54	0.00%	0.00%	0.00%	0.00%	3.52	6.16	9.02	0.00%	0.00%	0.00%	0.00%	3.96	6.48	6.38	0.00%	0.00%	0.00%
	cydX	1.678	8	22	0.00%	2.62	0.88	15.62	0.00%	0.00%	0.00%	0.00%	3.61	2.72	12.54	0.00%	0.00%	0.00%	0.00%	3.52	6.16	9.02	0.00%	0.00%	0.00%	0.00%	3.96	6.48	6.38	0.00%	0.00%	0.00%
cytochrome *bd*-II oxidase (AppCB)	appC	1.678	8	22	0.00%	2.62	0.88	15.62	0.00%	0.00%	0.00%	0.00%	3.61	2.72	12.54	0.00%	0.00%	0.00%	0.00%	3.52	6.16	9.02	0.00%	0.00%	0.00%	0.00%	3.96	6.48	6.38	0.00%	0.00%	0.00%
	appB	1.678	8	22	0.00%	2.62	0.88	15.62	0.00%	0.00%	0.00%	0.00%	3.61	2.72	12.54	0.00%	0.00%	0.00%	0.00%	3.52	6.16	9.02	0.00%	0.00%	0.00%	0.00%	3.96	6.48	6.38	0.00%	0.00%	0.00%
F_1 complex of ATP synthase	atpA	1.678	8	22	0.51%	2.62	0.88	15.62	0.07%	0.02%	0.42%	0.51%	3.61	2.72	12.54	0.10%	0.07%	0.34%	0.47%	3.52	6.16	9.02	0.09%	0.16%	0.23%	0.45%	3.96	6.48	6.38	0.11%	0.17%	0.17%
	atpC	1.678	8	22	0.05%	2.62	0.88	15.62	0.01%	0.00%	0.04%	0.05%	3.61	2.72	12.54	0.01%	0.01%	0.04%	0.05%	3.52	6.16	9.02	0.01%	0.02%	0.02%	0.05%	3.96	6.48	6.38	0.01%	0.02%	0.02%
	atpD	1.678	8	22	0.40%	2.62	0.88	15.62	0.05%	0.02%	0.32%	0.38%	3.61	2.72	12.54	0.07%	0.05%	0.25%	0.37%	3.52	6.16	9.02	0.07%	0.12%	0.18%	0.33%	3.96	6.48	6.38	0.08%	0.13%	0.12%
	atpG	1.678	8	22	0.10%	2.62	0.88	15.62	0.01%	0.00%	0.08%	0.09%	3.61	2.72	12.54	0.02%	0.01%	0.06%	0.08%	3.52	6.16	9.02	0.02%	0.03%	0.04%	0.07%	3.96	6.48	6.38	0.02%	0.03%	0.03%
	atpH	1.678	8	22	0.04%	2.62	0.88	15.62	0.01%	0.00%	0.03%	0.05%	3.61	2.72	12.54	0.01%	0.01%	0.03%	0.05%	3.52	6.16	9.02	0.01%	0.02%	0.02%	0.04%	3.96	6.48	6.38	0.01%	0.02%	0.02%
F_0 complex of ATP synthase	atpB	1.678	8	22	0.08%	2.62	0.88	15.62	0.01%	0.00%	0.07%	0.08%	3.61	2.72	12.54	0.02%	0.01%	0.05%	0.08%	3.52	6.16	9.02	0.02%	0.03%	0.04%	0.08%	3.96	6.48	6.38	0.02%	0.03%	0.03%
	atpE	1.678	8	22	0.15%	2.62	0.88	15.62	0.02%	0.01%	0.12%	0.15%	3.61	2.72	12.54	0.03%	0.02%	0.10%	0.15%	3.52	6.16	9.02	0.03%	0.05%	0.07%	0.15%	3.96	6.48	6.38	0.04%	0.06%	0.06%
	atpF	1.678	8	22	0.06%	2.62	0.88	15.62	0.01%	0.00%	0.05%	0.06%	3.61	2.72	12.54	0.01%	0.01%	0.04%	0.06%	3.52	6.16	9.02	0.01%	0.02%	0.03%	0.06%	3.96	6.48	6.38	0.01%	0.02%	0.02%

Table N5

					NQ381 (400)							NQ381 (500)							NQ381 (800)							NCM3722						
		Pathway stoichiometry				Flux through pathway			Protein mass allocated to pathway				Flux through pathway			Protein mass allocated to pathway				Flux through pathway			Protein mass allocated to pathway				Flux through pathway			Protein mass allocated to pathway		
Pathway or protein complex	Gene	Biomass ($S_{p,BM}$)	Fermentation ($S_{p,f}$)	Respiration ($S_{p,r}$)	Protein abundance (ϕ_p)	Biomass ($J_{p,BM}$)	Fermentation ($J_{p,f}$)	Respiration ($J_{p,r}$)	Biomass ($\phi_{p,BM}$)	Fermentation ($\phi_{p,f}$)	Respiration ($\phi_{p,r}$)	Protein abundance (ϕ_p)	Biomass ($J_{p,BM}$)	Fermentation ($J_{p,f}$)	Respiration ($J_{p,r}$)	Biomass ($\phi_{p,BM}$)	Fermentation ($\phi_{p,f}$)	Respiration ($\phi_{p,r}$)	Protein abundance (ϕ_p)	Biomass ($J_{p,BM}$)	Fermentation ($J_{p,f}$)	Respiration ($J_{p,r}$)	Biomass ($\phi_{p,BM}$)	Fermentation ($\phi_{p,f}$)	Respiration ($\phi_{p,r}$)	Protein abundance (ϕ_p)	Biomass ($J_{p,BM}$)	Fermentation ($J_{p,f}$)	Respiration ($J_{p,r}$)	Biomass ($\phi_{p,BM}$)	Fermentation ($\phi_{p,f}$)	Respiration ($\phi_{p,r}$)
					14.98%				4.94%	0.58%	9.47%	15.22%				5.98%	1.32%	7.92%	14.31%				5.70%	2.64%	5.96%	13.94%				6.47%	2.74%	4.73%
Lactose degradation	lacY	1	1	1	0.22%	1.54	0.11	0.73	0.14%	0.01%	0.07%	0.31%	2.12	0.35	0.59	0.22%	0.04%	0.06%	0.33%	2.07	0.79	0.41	0.21%	0.08%	0.04%	0.37%	2.33	0.84	0.29	0.25%	0.09%	0.03%
	lacZ	1	1	1	0.85%	1.54	0.11	0.73	0.55%	0.04%	0.26%	0.88%	2.12	0.35	0.59	0.61%	0.10%	0.17%	0.89%	2.07	0.79	0.41	0.57%	0.22%	0.11%	0.78%	2.33	0.84	0.29	0.53%	0.19%	0.07%
	glk	1	1	1	0.02%	1.54	0.11	0.73	0.01%	0.00%	0.01%	0.02%	2.12	0.35	0.59	0.01%	0.00%	0.00%	0.02%	2.07	0.79	0.41	0.01%	0.00%	0.00%	0.02%	2.33	0.84	0.29	0.01%	0.00%	0.00%
	pgm	1	1	1	0.03%	1.54	0.11	0.73	0.02%	0.00%	0.01%	0.00%	2.12	0.35	0.59	0.00%	0.00%	0.00%	0.00%	2.07	0.79	0.41	0.00%	0.00%	0.00%	0.00%	2.33	0.84	0.29	0.00%	0.00%	0.00%
	galM	1	1	1	0.08%	1.54	0.11	0.73	0.05%	0.00%	0.02%	0.07%	2.12	0.35	0.59	0.05%	0.01%	0.01%	0.08%	2.07	0.79	0.41	0.05%	0.02%	0.01%	0.08%	2.33	0.84	0.29	0.05%	0.02%	0.01%
	galK	1	1	1	0.18%	1.54	0.11	0.73	0.12%	0.01%	0.05%	0.20%	2.12	0.35	0.59	0.14%	0.02%	0.04%	0.22%	2.07	0.79	0.41	0.14%	0.05%	0.03%	0.13%	2.33	0.84	0.29	0.09%	0.03%	0.01%
	galT	1	1	1	0.03%	1.54	0.11	0.73	0.02%	0.00%	0.01%	0.03%	2.12	0.35	0.59	0.02%	0.00%	0.01%	0.03%	2.07	0.79	0.41	0.02%	0.01%	0.00%	0.06%	2.33	0.84	0.29	0.04%	0.02%	0.01%
	galE	1	1	1	0.15%	1.54	0.11	0.73	0.10%	0.01%	0.05%	0.16%	2.12	0.35	0.59	0.11%	0.02%	0.03%	0.29%	2.07	0.79	0.41	0.18%	0.07%	0.04%	0.26%	2.33	0.84	0.29	0.17%	0.06%	0.02%
Pentose phosphate pathway	zwf	0.79834	0.4	0.4	0.07%	1.23	0.044	0.292	0.05%	0.00%	0.01%	0.08%	1.69	0.14	0.236	0.07%	0.01%	0.01%	0.06%	1.65	0.316	0.164	0.05%	0.01%	0.00%	0.08%	1.86	0.336	0.116	0.07%	0.01%	0.00%
	pgl	0.79834	0.4	0.4	0.00%	1.23	0.044	0.292	0.00%	0.00%	0.00%	0.00%	1.69	0.14	0.236	0.00%	0.00%	0.00%	0.00%	1.65	0.316	0.164	0.00%	0.00%	0.00%	0.00%	1.86	0.336	0.116	0.00%	0.00%	0.00%
	gnd	0.79834	0.4	0.4	0.10%	1.23	0.044	0.292	0.08%	0.00%	0.02%	0.13%	1.69	0.14	0.236	0.10%	0.01%	0.01%	0.10%	1.65	0.316	0.164	0.08%	0.02%	0.01%	0.15%	1.86	0.336	0.116	0.12%	0.02%	0.01%
	rpe	0.79834	0.4	0.4	0.00%	1.23	0.044	0.292	0.00%	0.00%	0.00%	0.00%	1.69	0.14	0.236	0.00%	0.00%	0.00%	0.00%	1.65	0.316	0.164	0.00%	0.00%	0.00%	0.00%	1.86	0.336	0.116	0.00%	0.00%	0.00%
	rpiA	0.79834	0.4	0.4	0.03%	1.23	0.044	0.292	0.02%	0.00%	0.01%	0.07%	1.69	0.14	0.236	0.05%	0.00%	0.01%	0.06%	1.65	0.316	0.164	0.05%	0.01%	0.00%	0.10%	1.86	0.336	0.116	0.08%	0.01%	0.00%
	rpiB	0.79834	0.4	0.4	0.00%	1.23	0.044	0.292	0.00%	0.00%	0.00%	0.00%	1.69	0.14	0.236	0.00%	0.00%	0.00%	0.00%	1.65	0.316	0.164	0.00%	0.00%	0.00%	0.00%	1.86	0.336	0.116	0.00%	0.00%	0.00%
	tktA	0.44451	0.26	0.26	0.30%	0.68	0.0286	0.1898	0.17%	0.01%	0.05%	0.31%	0.94	0.091	0.1534	0.18%	0.02%	0.03%	0.34%	0.92	0.2054	0.1066	0.19%	0.04%	0.02%	0.33%	1.04	0.2184	0.0754	0.19%	0.04%	0.01%
	tktB	0.44451	0.26	0.26	0.00%	0.68	0.0286	0.1898	0.00%	0.00%	0.00%	0.00%	0.94	0.091	0.1534	0.00%	0.00%	0.00%	0.00%	0.92	0.2054	0.1066	0.00%	0.00%	0.00%	0.00%	1.04	0.2184	0.0754	0.00%	0.00%	0.00%
	talA	0.44451	0.26	0.26	0.00%	0.68	0.0286	0.1898	0.00%	0.00%	0.00%	0.00%	0.94	0.091	0.1534	0.00%	0.00%	0.00%	0.00%	0.92	0.2054	0.1066	0.00%	0.00%	0.00%	0.00%	1.04	0.2184	0.0754	0.00%	0.00%	0.00%
	talB	0.44451	0.26	0.26	0.15%	0.68	0.0286	0.1898	0.11%	0.00%	0.03%	0.16%	0.94	0.091	0.1534	0.13%	0.01%	0.02%	0.18%	0.92	0.2054	0.1066	0.13%	0.03%	0.02%	0.15%	1.04	0.2184	0.0754	0.12%	0.02%	0.01%
	tktA	0.13341	0.14	0.14	0.30%	0.21	0.0154	0.1022	0.05%	0.00%	0.02%	0.31%	0.28	0.049	0.0826	0.06%	0.01%	0.02%	0.34%	0.28	0.1106	0.0574	0.06%	0.02%	0.01%	0.33%	0.31	0.1176	0.0406	0.06%	0.02%	0.01%
	tktB	0.13341	0.14	0.14	0.00%	0.21	0.0154	0.1022	0.00%	0.00%	0.00%	0.00%	0.28	0.049	0.0826	0.00%	0.00%	0.00%	0.00%	0.28	0.1106	0.0574	0.00%	0.00%	0.00%	0.00%	0.31	0.1176	0.0406	0.00%	0.00%	0.00%
Glycolysis	pgi	1.1516	1.6	1.6	0.09%	1.77	0.176	1.168	0.05%	0.00%	0.03%	0.09%	2.44	0.56	0.944	0.05%	0.01%	0.02%	0.10%	2.38	1.264	0.656	0.05%	0.03%	0.02%	0.11%	2.68	1.344	0.464	0.06%	0.03%	0.01%
	pfkA	1.4898	1.86	1.86	0.06%	2.29	0.2046	1.3578	0.04%	0.00%	0.02%	0.06%	3.16	0.651	1.0974	0.04%	0.01%	0.01%	0.06%	3.08	1.4694	0.7626	0.04%	0.02%	0.01%	0.06%	3.47	1.5624	0.5394	0.04%	0.02%	0.01%
	pfkB	1.4898	1.86	1.86	0.00%	2.29	0.2046	1.3578	0.00%	0.00%	0.00%	0.00%	3.16	0.651	1.0974	0.00%	0.00%	0.00%	0.00%	3.08	1.4694	0.7626	0.00%	0.00%	0.00%	0.00%	3.47	1.5624	0.5394	0.00%	0.00%	0.00%
	fbaA	1.4898	1.86	1.86	0.32%	2.29	0.2046	1.3578	0.19%	0.02%	0.11%	0.35%	3.16	0.651	1.0974	0.22%	0.05%	0.08%	0.35%	3.08	1.4694	0.7626	0.20%	0.10%	0.05%	0.39%	3.47	1.5624	0.5394	0.24%	0.11%	0.04%
	fbaB	1.4898	1.86	1.86	0.00%	2.29	0.2046	1.3578	0.00%	0.00%	0.00%	0.00%	3.16	0.651	1.0974	0.00%	0.00%	0.00%	0.00%	3.08	1.4694	0.7626	0.00%	0.00%	0.00%	0.00%	3.47	1.5624	0.5394	0.00%	0.00%	0.00%
	tpiA	1.4898	1.86	1.86	0.12%	2.29	0.2046	1.3578	0.07%	0.01%	0.04%	0.15%	3.16	0.651	1.0974	0.10%	0.02%	0.03%	0.13%	3.08	1.4694	0.7626	0.08%	0.04%	0.02%	0.18%	3.47	1.5624	0.5394	0.11%	0.05%	0.02%
	gapA	3.082	3.86	3.86	1.19%	4.75	0.4246	2.8178	0.71%	0.06%	0.42%	1.29%	6.53	1.351	2.2774	0.83%	0.17%	0.29%	1.33%	6.38	3.0494	1.5826	0.77%	0.37%	0.19%	1.47%	7.18	3.2424	1.1194	0.92%	0.41%	0.14%
	pgk	3.082	3.86	3.86	0.30%	4.75	0.4246	2.8178	0.18%	0.02%	0.11%	0.31%	6.53	1.351	2.2774	0.20%	0.04%	0.07%	0.32%	6.38	3.0494	1.5826	0.18%	0.09%	0.05%	0.36%	7.18	3.2424	1.1194	0.22%	0.10%	0.04%
	gpmA	2.7146	3.86	3.86	0.15%	4.18	0.4246	2.8178	0.09%	0.01%	0.06%	0.15%	5.75	1.351	2.2774	0.09%	0.02%	0.04%	0.15%	5.62	3.0494	1.5826	0.08%	0.05%	0.02%	0.16%	6.33	3.2424	1.1194	0.10%	0.05%	0.02%
	gpmI	2.7146	3.86	3.86	0.08%	4.18	0.4246	2.8178	0.04%	0.00%	0.03%	0.08%	5.75	1.351	2.2774	0.05%	0.01%	0.02%	0.10%	5.62	3.0494	1.5826	0.05%	0.03%	0.01%	0.11%	6.33	3.2424	1.1194	0.06%	0.03%	0.01%
	eno	2.7146	3.86	3.86	0.63%	4.18	0.4246	2.8178	0.36%	0.04%	0.24%	0.70%	5.75	1.351	2.2774	0.43%	0.10%	0.17%	0.75%	5.62	3.0494	1.5826	0.41%	0.22%	0.12%	0.83%	6.33	3.2424	1.1194	0.49%	0.25%	0.09%
	pykF	1.8813	3.86	3.86	0.15%	2.90	0.4246	2.8178	0.07%	0.01%	0.07%	0.15%	3.99	1.351	2.2774	0.08%	0.03%	0.05%	0.18%	3.89	3.0494	1.5826	0.08%	0.06%	0.03%	0.21%	4.38	3.2424	1.1194	0.11%	0.08%	0.03%
	pykA	1.8813	3.86	3.86	0.18%	2.90	0.4246	2.8178	0.08%	0.01%	0.08%	0.13%	3.99	1.351	2.2774	0.07%	0.02%	0.04%	0.06%	3.89	3.0494	1.5826	0.03%	0.02%	0.01%	0.06%	4.38	3.2424	1.1194	0.03%	0.02%	0.01%
	aceE	1.1852	3.86	3.86	0.30%	1.83	0.4246	2.8178	0.11%	0.03%	0.17%	0.32%	2.51	1.351	2.2774	0.13%	0.07%	0.12%	0.34%	2.45	3.0494	1.5826	0.12%	0.15%	0.08%	0.41%	2.76	3.2424	1.1194	0.16%	0.19%	0.06%
	aceF	1.1852	3.86	3.86	0.21%	1.83	0.4246	2.8178	0.08%	0.02%	0.12%	0.24%	2.51	1.351	2.2774	0.10%	0.05%	0.09%	0.24%	2.45	3.0494	1.5826	0.08%	0.10%	0.05%	0.25%	2.76	3.2424	1.1194	0.10%	0.11%	0.04%
	lpdA	1.1852	3.86	3.86	0.63%	1.83	0.4246	2.8178	0.15%	0.03%	0.23%	0.61%	2.51	1.351	2.2774	0.18%	0.10%	0.17%	0.56%	2.45	3.0494	1.5826	0.16%	0.20%	0.10%	0.52%	2.76	3.2424	1.1194	0.18%	0.21%	0.07%
	pta	0	3.86	0	0.10%	0.00	0.4246	0	0.00%	0.10%	0.00%	0.10%	0.00	1.351	0	0.00%	0.10%	0.00%	0.10%	0.00	3.0494	0	0.00%	0.10%	0.00%	0.10%	0.00	3.2424	0	0.00%	0.10%	0.00%
	ackA	0	3.86	0	0.06%	0.00	0.4246	0	0.00%	0.06%	0.00%	0.07%	0.00	1.351	0	0.00%	0.07%	0.00%	0.06%	0.00	3.0494	0	0.00%	0.06%	0.00%	0.00%	0.00	3.2424	0	0.00%	0.00%	0.00%
TCA	gltA	0.26489	0	3.86	0.88%	0.41	0	2.8178	0.11%	0.00%	0.77%	0.80%	0.56	0	2.2774	0.16%	0.00%	0.65%	0.61%	0.55	0	1.5826	0.16%	0.00%	0.46%	0.48%	0.62	0	1.1194	0.17%	0.00%	0.31%
	acnA	0.26489	0	3.86	0.03%	0.41	0	2.8178	0.00%	0.00%	0.03%	0.00%	0.56	0	2.2774	0.00%	0.00%	0.00%	0.00%	0.55	0	1.5826	0.00%	0.00%	0.00%	0.00%	0.62	0	1.1194	0.00%	0.00%	0.00%
	acnB	0.26489	0	3.86	0.92%	0.41	0	2.8178	0.12%	0.00%	0.80%	0.84%	0.56	0	2.2774	0.17%	0.00%	0.68%	0.66%	0.55	0	1.5826	0.17%	0.00%	0.49%	0.57%	0.62	0	1.1194	0.20%	0.00%	0.37%
	icd	0.26489	0	3.86	1.55%	0.41	0	2.8178	0.20%	0.00%	1.36%	1.55%	0.56	0	2.2774	0.31%	0.00%	1.25%	1.31%	0.55	0	1.5826	0.34%	0.00%	0.97%	1.39%	0.62	0	1.1194	0.50%	0.00%	0.90%
	sucA	0	0	3.86	0.33%	0.00	0	2.8178	0.00%	0.00%	0.33%	0.36%	0.00	0	2.2774	0.00%	0.00%	0.36%	0.29%	0.00	0	1.5826	0.00%	0.00%	0.29%	0.25%	0.00	0	1.1194	0.00%	0.00%	0.25%
	sucB	0	0	3.86	0.38%	0.00	0	2.8178	0.00%	0.00%	0.38%	0.39%	0.00	0	2.2774	0.00%	0.00%	0.39%	0.35%	0.00	0	1.5826	0.00%	0.00%	0.35%	0.30%	0.00	0	1.1194	0.00%	0.00%	0.30%
	lpdA	0	0	3.86	0.63%	0.00	0	2.8178	0.00%	0.00%	0.23%	0.61%	0.00	0	2.2774	0.00%	0.00%	0.17%	0.56%	0.00	0	1.5826	0.00%	0.00%	0.10%	0.52%	0.00	0	1.1194	0.00%	0.00%	0.07%
	sucC	0	0	3.86	0.52%	0.00	0	2.8178	0.00%	0.00%	0.52%	0.49%	0.00	0	2.2774	0.00%	0.00%	0.49%	0.38%	0.00	0	1.5826	0.00%	0.00%	0.38%	0.30%	0.00	0	1.1194	0.00%	0.00%	0.30%
	sucD	0	0	3.86	0.36%	0.00	0	2.8178	0.00%	0.00%	0.36%	0.35%	0.00	0	2.2774	0.00%	0.00%	0.35%	0.28%	0.00	0	1.5826	0.00%	0.00%	0.28%	0.22%	0.00	0	1.1194	0.00%	0.00%	0.22%
	sdhA	0	0	3.86	0.33%	0.00	0	2.8178	0.00%	0.00%	0.33%	0.30%	0.00	0	2.2774	0.00%	0.00%	0.30%	0.29%	0.00	0	1.5826	0.00%	0.00%	0.29%	0.24%	0.00	0	1.1194	0.00%	0.00%	0.24%
	sdhB	0	0	3.86	0.16%	0.00	0	2.8178	0.00%	0.00%	0.16%	0.15%	0.00	0	2.2774	0.00%	0.00%	0.15%	0.13%	0.00	0	1.5826	0.00%	0.00%	0.13%	0.11%	0.00	0	1.1194	0.00%	0.00%	0.11%
	sdhC	0	0	3.86	0.00%	0.00	0	2.8178	0.00%	0.00%	0.00%	0.00%	0.00	0	2.2774	0.00%	0.00%	0.00%	0.00%	0.00	0	1.5826	0.00%	0.00%	0.00%	0.00%	0.00	0	1.1194	0.00%	0.00%	0.00%
	sdhD	0	0	3.86	0.00%	0.00	0	2.8178	0.00%	0.00%	0.00%	0.00%	0.00	0	2.2774	0.00%	0.00%	0.00%	0.00%	0.00	0	1.5826	0.00%	0.00%	0.00%	0.00%	0.00	0	1.1194	0.00%	0.00%	0.00%
	fumA	0	0	3.86	0.24%	0.00	0	2.8178	0.00%	0.00%	0.24%	0.21%	0.00	0	2.2774	0.00%	0.00%	0.21%	0.17%	0.00	0	1.5826	0.00%	0.00%	0.17%	0.13%	0.00	0	1.1194	0.00%	0.00%	0.13%
	fumB	0	0	3.86	0.00%	0.00	0	2.8178	0.00%	0.00%	0.00%	0.00%	0.00	0	2.2774	0.00%	0.00%	0.00%	0.00%	0.00	0	1.5826	0.00%	0.00%	0.00%	0.00%	0.00	0	1.1194	0.00%	0.00%	0.00%
	fumC	0	0	3.86	0.00%	0.00	0	2.8178	0.00%	0.00%	0.00%	0.00%	0.00	0	2.2774	0.00%	0.00%	0.00%	0.00%	0.00	0	1.5826	0.00%	0.00%	0.00%	0.00%	0.00	0	1.1194	0.00%	0.00%	0.00%
	mdh	0	0	3.86	0.45%	0.00	0	2.8178	0.00%	0.00%	0.45%	0.45%	0.00	0	2.2774	0.00%	0.00%	0.45%	0.41%	0.00	0	1.5826	0.00%	0.00%	0.41%	0.39%	0.00	0	1.1194	0.00%	0.00%	0.39%
	ppc	0.70379	0	0	0.16%	1.08	0	0	0.16%	0.00%	0.00%	0.18%	1.49	0	0	0.18%	0.00%	0.00%	0.18%	1.46	0	0	0.18%	0.00%	0.00%	0.19%	1.64	0	0	0.19%	0.00%	0.00%
NADH:ubiquinone oxidoreductase I (NDH-1)	nuoA	5.8639	8.54	22.06	0.02%	9.03	0.9394	16.1038	0.01%	0.00%	0.01%	0.02%	12.43	2.989	13.0154	0.01%	0.00%	0.01%	0.02%	12.14	6.7466	9.0446	0.01%	0.00%	0.00%	0.01%	13.66	7.1736	6.3974	0.01%	0.00%	0.00%
	nuoB	5.8639	8.54	22.06	0.04%	9.03	0.9394	16.1038	0.01%	0.00%	0.03%	0.04%	12.43	2.989	13.0154	0.02%	0.00%	0.02%	0.03%	12.14	6.7466	9.0446	0.02%	0.01%	0.01%	0.03%	13.66	7.1736	6.3974	0.02%	0.01%	0.01%
	nuoC	5.8639	8.54	22.06	0.08%	9.03	0.9394	16.1038	0.03%	0.00%	0.05%	0.07%	12.43	2.989	13.0154	0.03%	0.01%	0.03%	0.06%	12.14	6.7466	9.0446	0.03%	0.02%	0.02%	0.06%	13.66	7.1736	6.3974	0.03%	0.01%	0.01%
	nuoE	5.8639	8.54	22.06	0.03%	9.03	0.9394	16.1038	0.01%	0.00%	0.02%	0.03%	12.43	2.989	13.0154	0.01%	0.00%	0.01%	0.03%	12.14	6.7466	9.0446	0.01%	0.01%	0.01%	0.02%	13.66	7.1736	6.3974	0.01%	0.01%	0.01%
	nuoF	5.8639	8.54	22.06	0.05%	9.03	0.9394	16.1038	0.02%	0.00%	0.03%	0.05%	12.43	2.989	13.0154	0.02%	0.01%	0.02%	0.04%	12.14	6.7466	9.0446	0.02%	0.01%	0.01%	0.04%	13.66	7.1736	6.3974	0.02%	0.01%	0.01%
	nuoG	5.8639	8.54	22.06	0.12%	9.03	0.9394	16.1038	0.04%	0.00%	0.07%	0.12%	12.43	2.989	13.0154	0.05%	0.01%	0.05%	0.10%	12.14	6.7466	9.0446	0.04%	0.02%	0.03%	0.09%	13.66	7.1736	6.3974	0.04%	0.02%	0.02%
	nuoH	5.8639	8.54	22.06	0.02%	9.03	0.9394	16.1038	0.01%	0.00%	0.01%	0.02%	12.43	2.989	13.0154	0.01%	0.00%	0.01%	0.02%	12.14	6.7466	9.0446	0.01%	0.00%	0.01%	0.02%	13.66	7.1736	6.3974	0.01%	0.00%	0.00%
	nuoI	5.8639	8.54	22.06	0.02%	9.03	0.9394	16.1038	0.01%	0.00%	0.01%	0.02%	12.43	2.989	13.0154	0.01%	0.00%	0.01%	0.02%	12.14	6.7466	9.0446	0.01%	0.00%	0.01%	0.01%	13.66	7.1736	6.3974	0.01%	0.00%	0.00%
	nuoJ	5.8639	8.54	22.06	0.01%	9.03	0.9394	16.1038	0.00%	0.00%	0.01%	0.01%	12.43	2.989	13.0154	0.00%	0.00%	0.00%	0.01%	12.14	6.7466	9.0446	0.00%	0.00%	0.00%	0.01%	13.66	7.1736	6.3974	0.00%	0.00%	0.00%
	nuoK	5.8639	8.54	22.06	0.01%	9.03	0.9394	16.1038	0.00%	0.00%	0.00%	0.01%	12.43	2.989	13.0154	0.00%	0.00%	0.00%	0.01%	12.14	6.7466	9.0446	0.00%	0.00%	0.00%	0.00%	13.66	7.1736	6.3974	0.00%	0.00%	0.00%
	nuoL	5.8639	8.54	22.06	0.03%	9.03	0.9394	16.1038	0.01%	0.00%	0.02%	0.03%	12.43	2.989	13.0154	0.01%	0.00%	0.02%	0.03%	12.14	6.7466	9.0446	0.01%	0.01%	0.01%	0.03%	13.66	7.1736	6.3974	0.01%	0.01%	0.01%
	nuoM	5.8639	8.54	22.06	0.03%	9.03	0.9394	16.1038	0.01%	0.00%	0.02%	0.03%	12.43	2.989	13.0154	0.01%	0.00%	0.01%	0.03%	12.14	6.7466	9.0446	0.01%	0.01%	0.01%	0.02%	13.66	7.1736	6.3974	0.01%	0.01%	0.01%
	nuoN	5.8639	8.54	22.06	0.04%	9.03	0.9394	16.1038	0.01%	0.00%	0.02%	0.03%	12.43	2.989	13.0154	0.02%	0.00%	0.02%	0.03%	12.14	6.7466	9.0446	0.01%	0.01%	0.01%	0.03%	13.66	7.1736	6.3974	0.01%	0.01%	0.01%
NADH:ubiquinone oxidoreductase II (NDH-2)	ndh	5.8639	8.54	22.06	0.00%	9.03	0.9394	16.1038	0.00%	0.00%	0.00%	0.00%	12.43	2.989	13.0154	0.00%	0.00%	0.00%	0.03%	12.14	6.7466	9.0446	0.01%	0.01%	0.01%	0.00%	13.66	7.1736	6.3974	0.00%	0.00%	0.00%
cytochrome *bo* oxidase (CyoABCD)	cyoA	5.8639	8.54	22.06	0.00%	9.03	0.9394	16.1038	0.00%	0.00%	0.00%	0.03%	12.43	2.989	13.0154	0.01%	0.00%	0.01%	0.03%	12.14	6.7466	9.0446	0.01%	0.01%	0.01%	0.03%	13.66	7.1736	6.3974	0.02%	0.01%	0.01%
	cyoB	5.8639	8.54	22.06	0.00%	9.03	0.9394	16.1038	0.00%	0.00%	0.00%	0.00%	12.43	2.989	13.0154	0.00%	0.00%	0.00%	0.00%	12.14	6.7466	9.0446	0.00%	0.00%	0.00%	0.00%	13.66	7.1736	6.3974	0.00%	0.00%	0.00%
	cyoC	5.8639	8.54	22.06	0.00%	9.03	0.9394	16.1038	0.00%	0.00%	0.00%	0.00%	12.43	2.989	13.0154	0.00%	0.00%	0.00%	0.00%	12.14	6.7466	9.0446	0.00%	0.00%	0.00%	0.00%	13.66	7.1736	6.3974	0.00%	0.00%	0.00%
	cyoD	5.8639	8.54	22.06	0.00%	9.03	0.9394	16.1038	0.00%	0.00%	0.00%	0.00%	12.43	2.989	13.0154	0.00%	0.00%	0.00%	0.00%	12.14	6.7466	9.0446	0.00%	0.00%	0.00%	0.00%	13.66	7.1736	6.3974	0.00%	0.00%	0.00%
cytochrome *bd*-I oxidase (CydABX)	cydA	5.8639	8.54	22.06	0.00%	9.03	0.9394	16.1038	0.00%	0.00%	0.00%	0.00%	12.43	2.989	13.0154	0.00%	0.00%	0.00%	0.00%	12.14	6.7466	9.0446	0.00%	0.00%	0.00%	0.00%	13.66	7.1736	6.3974	0.00%	0.00%	0.00%
	cydB	5.8639	8.54	22.06	0.00%	9.03	0.9394	16.1038	0.00%	0.00%	0.00%	0.00%	12.43	2.989	13.0154	0.00%	0.00%	0.00%	0.00%	12.14	6.7466	9.0446	0.00%	0.00%	0.00%	0.00%	13.66	7.1736	6.3974	0.00%	0.00%	0.00%
	cydX	5.8639	8.54	22.06	0.00%	9.03	0.9394	16.1038	0.00%	0.00%	0.00%	0.00%	12.43	2.989	13.0154	0.00%	0.00%	0.00%	0.00%	12.14	6.7466	9.0446	0.00%	0.00%	0.00%	0.00%	13.66	7.1736	6.3974	0.00%	0.00%	0.00%
cytochrome *bd*-II oxidase (AppCB)	appC	5.8639	8.54	22.06	0.00%	9.03	0.9394	16.1038	0.00%	0.00%	0.00%	0.00%	12.43	2.989	13.0154	0.00%	0.00%	0.00%	0.00%	12.14	6.7466	9.0446	0.00%	0.00%	0.00%	0.00%	13.66	7.1736	6.3974	0.00%	0.00%	0.00%
	appB	5.8639	8.54	22.06	0.00%	9.03	0.9394	16.1038	0.00%	0.00%	0.00%	0.00%	12.43	2.989	13.0154	0.00%	0.00%	0.00%	0.00%	12.14	6.7466	9.0446	0.00%	0.00%	0.00%	0.00%	13.66	7.1736	6.3974	0.00%	0.00%	0.00%
F_1 complex of ATP synthase	atpA	5.8639	8.54	22.06	0.51%	9.03	0.9394	16.1038	0.18%	0.02%	0.32%	0.51%	12.43	2.989	13.0154	0.22%	0.05%	0.23%	0.47%	12.14	6.7466	9.0446	0.21%	0.11%	0.15%	0.45%	13.66	7.1736	6.3974	0.23%	0.12%	0.11%
	atpC	5.8639	8.54	22.06	0.05%	9.03	0.9394	16.1038	0.02%	0.00%	0.03%	0.05%	12.43	2.989	13.0154	0.02%	0.01%	0.02%	0.05%	12.14	6.7466	9.0446	0.02%	0.01%	0.02%	0.05%	13.66	7.1736	6.3974	0.02%	0.01%	0.01%
	atpD	5.8639	8.54	22.06	0.40%	9.03	0.9394	16.1038	0.14%	0.01%	0.24%	0.38%	12.43	2.989	13.0154	0.17%	0.04%	0.17%	0.37%	12.14	6.7466	9.0446	0.16%	0.09%	0.12%	0.33%	13.66	7.1736	6.3974	0.16%	0.09%	0.08%
	atpG	5.8639	8.54	22.06	0.10%	9.03	0.9394	16.1038	0.03%	0.00%	0.06%	0.09%	12.43	2.989	13.0154	0.04%	0.01%	0.04%	0.08%	12.14	6.7466	9.0446	0.03%	0.02%	0.03%	0.07%	13.66	7.1736	6.3974	0.04%	0.02%	0.02%
	atpH	5.8639	8.54	22.06	0.04%	9.03	0.9394	16.1038	0.01%	0.00%	0.03%	0.05%	12.43	2.989	13.0154	0.02%	0.00%	0.02%	0.05%	12.14	6.7466	9.0446	0.02%	0.01%	0.02%	0.04%	13.66	7.1736	6.3974	0.02%	0.01%	0.01%
F_0 complex of ATP synthase	atpB	5.8639	8.54	22.06	0.08%	9.03	0.9394	16.1038	0.03%	0.00%	0.05%	0.08%	12.43	2.989	13.0154	0.03%	0.01%	0.04%	0.08%	12.14	6.7466	9.0446	0.03%	0.02%	0.03%	0.08%	13.66	7.1736	6.3974	0.04%	0.02%	0.02%
	atpE	5.8639	8.54	22.06	0.15%	9.03	0.9394	16.1038	0.05%	0.01%	0.09%	0.15%	12.43	2.989	13.0154	0.06%	0.02%	0.07%	0.15%	12.14	6.7466	9.0446	0.06%	0.04%	0.05%	0.15%	13.66	7.1736	6.3974	0.07%	0.04%	0.04%
	atpF	5.8639	8.54	22.06	0.06%	9.03	0.9394	16.1038	0.02%	0.00%	0.04%	0.06%	12.43	2.989	13.0154	0.03%	0.01%	0.03%	0.06%	12.14	6.7466	9.0446	0.03%	0.01%	0.02%	0.06%	13.66	7.1736	6.3974	0.03%	0.02%	0.01%